MARTIN MARIETTA ENERGY SYSTEMS LIBRARIES
3 4456 0056754 4

ORNL/TM-9788

ornl

OAK RIDGE NATIONAL LABORATORY

MARTIN MARIETTA

ICRF Wave Propagation and Absorption in Tokamak and Mirror Magnetic Fields: A Full-Wave Calculation

E. F. Jaeger
D. B. Batchelor
H. Weitzner
J. H. Whealton

OAK RIDGE NATIONAL LABORATORY
CENTRAL RESEARCH LIBRARY
CIRCULATION SECTION
4500N ROOM 175
LIBRARY LOAN COPY
DO NOT TRANSFER TO ANOTHER PERSON
If you wish someone else to see this report, send in name with report and the library will arrange a loan.

OPERATED BY
MARTIN MARIETTA ENERGY SYSTEMS, INC.
FOR THE UNITED STATES
DEPARTMENT OF ENERGY

Printed in the United States of America. Available from
National Technical Information Service
U.S. Department of Commerce
5285 Port Royal Road, Springfield, Virginia 22161
NTIS price codes—Printed Copy: A05; Microfiche A01

This report was prepared as an account of work sponsored by an agency of the United States Government. Neither the United States Government nor any agency thereof, nor any of their employees, makes any warranty, express or implied, or assumes any legal liability or responsibility for the accuracy, completeness, or usefulness of any information, apparatus, product, or process disclosed, or represents that its use would not infringe privately owned rights. Reference herein to any specific commercial product, process, or service by trade name, trademark, manufacturer, or otherwise, does not necessarily constitute or imply its endorsement, recommendation, or favoring by the United States Government or any agency thereof. The views and opinions of authors expressed herein do not necessarily state or reflect those of the United States Government or any agency thereof.

ORNL/TM-9788
Dist. Category UC-20 g

Fusion Energy Division

ICRF WAVE PROPAGATION AND ABSORPTION IN TOKAMAK AND MIRROR MAGNETIC FIELDS: A FULL-WAVE CALCULATION

E. F. Jaeger
D. B. Batchelor
H. Weitzner*
J. H. Whealton

Date Published - January 1986

*Courant Institute of Mathematical Sciences, New York University, New York, New York 10012.

Prepared by the
OAK RIDGE NATIONAL LABORATORY
Oak Ridge, Tennessee 37831
operated by
MARTIN MARIETTA ENERGY SYSTEMS, INC.
for the
U.S. DEPARTMENT OF ENERGY
under Contract No. DE-AC05-84OR21400

MARTIN MARIETTA ENERGY SYSTEMS LIBRARIES
3 4456 0056754 4

CONTENTS

ABSTRACT..... v

1. INTRODUCTION..... 1

2. COLD PLASMA THEORY..... 3

2.1 WAVE EQUATION..... 5

2.2 LOCAL DISPERSION RELATION..... 5

3. DIELECTRIC TENSOR REPRESENTATION..... 8

4. THE STRAIGHT TOKAMAK WITH POLOIDAL FIELD..... 10

4.1 WAVE EQUATION FOR THE TOKAMAK..... 12

4.2 LOCAL ENERGY DEPOSITION AND ANTENNA IMPEDANCE IN THE TOKAMAK..... 16

4.3 ANTENNA CURRENT FOR THE TOKAMAK..... 20

5. NUMERICAL RESULTS FOR THE TOKAMAK..... 23

5.1 TWO-ION HYBRID RESONANCE..... 23

5.2 FUNDAMENTAL ION CYCLOTRON RESONANCE IN TOKAMAKS..... 38

6. THE POLOIDALLY SYMMETRIC MAGNETIC MIRROR..... 45

6.1 WAVE EQUATIONS FOR THE MIRROR..... 47

6.2 MODEL MIRROR MAGNETIC FIELD..... 49

6.3 ANTENNA CURRENT FOR THE POLOIDALLY SYMMETRIC MIRROR..... 52

6.4 LOCAL ENERGY DEPOSITION AND ANTENNA IMPEDANCE IN THE MIRROR..... 53

7. NUMERICAL RESULTS FOR THE MAGNETIC MIRROR..... 55

8. DISCUSSION..... 59

REFERENCES..... 61

ABSTRACT

Global solutions for the ion cyclotron resonant frequency (ICRF) wave fields in a straight tokamak with rotational transform and in a poloidally symmetric mirror are calculated in the cold plasma limit. The component of the wave electric field parallel to $\vec{B}$ is assumed zero. Symmetry in each problem allows Fourier decomposition in one ignorable coordinate, and the remaining set of two coupled, two-dimensional partial differential equations is solved by finite differencing. Energy absorption and antenna impedance are calculated using a simple collisional absorption model. When large gradients in $|B|$ along $\vec{B}$ are present in either geometry, ICRF heating at the fundamental ion cyclotron resonance is observed. For the mirror, such gradients are always present. But for the tokamak, the rotational transform must be large enough that $\vec{B} \cdot \nabla B \gtrsim O(1)$. For smaller transforms more typical of real tokamaks, only heating at the two-ion hybrid resonance is observed. This suggests that direct resonant absorption at the fundamental ion cyclotron resonance may be possible in stellarators where $\vec{B} \cdot \nabla B \sim O(1)$ naturally.

1. INTRODUCTION

For many laboratory plasmas in which low-frequency, long-wavelength ICRF fields are present, the geometrical optics assumptions are not valid. In these cases, global solutions for the wave fields are needed to calculate energy absorption profiles and antenna loading. Such solutions, however, involve inverting the highly singular operator $-\nabla \times \nabla \times \vec{E}$ and may lead to numerical difficulties. To make this problem more tractable it has become standard with some authors [1-5] to assume that the high conductivity of the plasma along field lines shorts out the component of the wave electric field parallel to $\vec{B}$; that is, $\vec{B} \cdot \vec{E} = 0$ on the time scale of the wave. For ion cyclotron frequencies this is a good approximation. Likewise, further simplification occurs when the geometry allows Fourier decomposition in one or more ignorable coordinates, thus reducing the dimensionality of the system to only one or two spatial dimensions. With these assumptions, full-wave solutions in the cold plasma limit have been carried out by several authors [1-7]. McVey [6] treats the mirror problem assuming both poloidal and axial symmetry, thus reducing the problem to one radial dimension. However, Phillips and Todd [7] point out the importance of retaining axial inhomogeneity in the mirror field and also the possible importance of parallel electric fields. Itoh et al. [1] treat a straight tokamak with axial symmetry and collisional absorption, but they neglect the poloidal component of the magnetic field. As the calculations in this paper show, however, the effect of the poloidal field on $\vec{B} \cdot \nabla B$ in the tokamak is to allow energy absorption at the fundamental ion cyclotron resonance. Colestock and Kashuba [2] also treat the straight tokamak without poloidal field, but

they attempt to model mode conversion to ion Bernstein waves as the mechanism for wave damping and energy absorption. Work in progress by Elet et al. [4] and Appert et al. [5] attempts to include both poloidal magnetic field and the full geometrical effect of toroidal curvature in the tokamak.

In this paper we extend the full-wave treatments of McVey [6] and Itoh et al. [1] to include both radial and axial variations in $\vec{B}$ for the mirror and to include the poloidal magnetic field B_θ for the tokamak. Energy absorption profiles and antenna impedance are calculated using the simple collisional absorption model of Itoh et al. [1]. By including the effect of the poloidal field, we allow energy absorption at the fundamental ion cyclotron resonance in tokamak as well as mirror geometry. Such absorption in a tokamak requires a rotational transform large enough to produce a significant gradient in $|B|$ along $\vec{B}$, i.e., $\vec{B} \cdot \nabla B$. For the case of zero poloidal field as treated by Itoh et al., the gradient in $|B|$ along $\vec{B}$ is zero and only heating at the two-ion hybrid resonance is observed. These results support the contention [7-9] that large gradients in $|B|$ along $\vec{B}$ in the stellarator may lead to ICRF heating at the fundamental of the ion cyclotron frequency in that more complicated geometry.

In Section 2 we review the assumptions of cold plasma theory leading to the cold plasma dielectric tensor, wave equation, and dispersion relation. Section 3 explains the decomposition of the dielectric tensor into components along unit tensors made up of an orthogonal set of unit vectors describing generalized flux coordinates. In Section 4 the special case of tokamak geometry, including an arbitrary poloidal magnetic field, is considered. The wave equations are shown to reduce exactly to those of Itoh et al. [1] in the limit that B_θ approaches zero.

Expressions for the energy deposition rate and antenna impedance including the poloidal magnetic field are derived in Section 4.2. Section 5 describes numerical results for the tokamak, including an explicit example in which energy is absorbed at the fundamental ion cyclotron resonance. In Section 6, the special case of mirror geometry including both radial and axial variations in $\vec{B}$ is considered, and Section 7 describes numerical results for a model mirror field. Finally, Section 8 discusses the implications and possible extensions of these calculations.

2. COLD PLASMA THEORY

Combining Maxwell's equations with the Lorentz force equations gives the equations of cold plasma theory [10],

$$\nabla \times \vec{E} = i\omega\vec{B} \ , \tag{1}$$

$$\nabla \times \vec{H} = \vec{J}_{ext} - i\omega\left(\varepsilon_0 \overleftrightarrow{K} \cdot \vec{E}\right) \ , \tag{2}$$

$$\nabla \cdot \left(\varepsilon_0 \overleftrightarrow{K} \cdot \vec{E}\right) = \rho_{ext} \ , \tag{3}$$

$$\nabla \cdot \vec{B} = 0 \ , \tag{4}$$

where time-harmonic dependence for the wave fields has been assumed with the form $e^{-i\omega t}$. In (1)-(4) $\overleftrightarrow{K}$ is the cold plasma dielectric tensor. In the coordinate system where the applied magnetic field $\vec{B}_0$ is in the z direction, $\overleftrightarrow{K}$ can be written as [10]

$$\overleftrightarrow{K} = \overleftrightarrow{I} + \frac{i}{\omega\varepsilon_0}\overleftrightarrow{\sigma} = \begin{bmatrix} K_\perp & -iK_x & 0 \\ iK_x & K_\perp & 0 \\ 0 & 0 & K_\parallel \end{bmatrix} \ , \tag{5}$$

where $\overleftrightarrow{I}$ is the identity tensor, $\overleftrightarrow{\sigma}$ is the cold plasma conductivity tensor, and

$$K_{\perp} = 1 - \sum_j \frac{\omega_{pj}^2}{\omega^2 - \Omega_j^2} ,$$

$$K_x = \sum_j \frac{\Omega_j}{\omega} \frac{\omega_{pj}^2}{\omega^2 - \Omega_j^2} , \tag{6}$$

$$K_{\parallel} = 1 - \sum_j \frac{\omega_{pj}^2}{\omega^2} .$$

In (6), $\omega_{pj}^2 = nq_j^2/(m_j\varepsilon_0)$; $\Omega_j = q_jB_0/m_j$; and m_j and q_j are the mass and charge respectively for the j<u>th</u> species; n is the plasma density; $\vec{E} = \vec{D}/\varepsilon_0$ and $\vec{H} = \vec{B}/\mu_0$ are the wave electric and magnetic field stength vectors, respectively, where $\varepsilon_0 = 8.85 \times 10^{-12}$ $F\cdot m^{-1}$ is the permittivity constant and $\mu_0 = 1.26 \times 10^{-6}$ $H\cdot m^{-1}$ is the permeability constant. $\vec{\rho}_{ext}$ and $\vec{J}_{ext}$ are the external (excluding plasma polarization effects) charge density and current density, respectively.

The approximate effect of collisions can be included in (1)-(6) by adding a collisional damping term to the Lorentz force equation [1]:

$$m_j \frac{\partial \vec{v}_j}{\partial t} = q_j\left(\vec{E} + \vec{v}_j \times \vec{B}\right) - \nu_j m_j \vec{v}_j ,$$

where $\vec{v}_j$ is the particle velocity and ν_j is the collision frequency. Assuming $v_j \propto e^{-i\omega t}$ now gives

$$-m_j\left(1 + i\,\frac{\nu_j}{\omega}\right) i\omega\vec{v}_j = q_j\left(\vec{E} + \vec{v}_j \times \vec{B}\right) .$$

Thus we see that the effect of collisions can be included in the cold plasma theory by replacing the mass m_j with $m_j^* = m_j(1 + i\nu_j/\omega)$ in (1)-(6). Note that for ν_j positive, the particle motion is damped.

2.1 WAVE EQUATION

To write the wave equation for the electric field, take the curl of (1) and use (2) to eliminate $\vec{B}$. We find

$$-\nabla \times \nabla \times \vec{E} + \frac{\omega^2}{c^2}\overleftrightarrow{K} \cdot \vec{E} = -i\omega\mu_0\vec{J}_{ext} , \tag{7}$$

where c is the speed of light in vacuum, $c = 1/\sqrt{\varepsilon_0\mu_0} \sim 3 \times 10^8$ m/s.

Boundary conditions appropriate to the solution of (7) are that the tangential component of $\vec{E}$ should vanish at the surface of a perfect conductor along with the normal component of $\vec{B}$. Note that solving (7) automatically guarantees a solution to (3) because the divergence of (7) with conservation of change, $\dot{\rho} = -\nabla \cdot \vec{J}$, gives (3) exactly.

2.2 LOCAL DISPERSION RELATION

In the local approximation, $\vec{E}(\vec{x}) = \vec{E}\, e^{i\vec{k}\cdot\vec{x}}$ so that $\nabla \to i\vec{k}$ and (7) gives the cold plasma dispersion relation. Assuming without loss of generality that $\vec{k}$ lies in the x-z plane, $\vec{k} = k_\perp\hat{x} + k_\parallel\hat{z}$ with $\vec{B} = B\hat{z}$, a homogeneous solution to (7) exists when [10]

$$\left(\frac{\omega^2}{c^2} K_{\parallel} - k_{\perp}^2\right)\left[\left(\frac{\omega^2}{c^2} K_{\perp} - k_{\parallel}^2\right)\left(\frac{\omega^2}{c^2} K_{\perp} - k^2\right) - \frac{\omega^4}{c^4} K_x^2\right]$$

$$- k_{\perp}^2 k_{\parallel}^2 \left(\frac{\omega^2}{c^2} K_{\perp} - k^2\right) = 0 \ . \tag{8}$$

This is the cold plasma dispersion relation. In the low-frequency limit when $\omega \ll \omega_{pj}$, then $|K_{\parallel}| \gg |K_{\perp}| \sim |K_x|$ and we need only keep the term proportional to $K_{\parallel}$ in (8). Solving for $k_{\perp}$ then gives [11]

$$k_{\perp}^2 = \frac{\left(\frac{\omega^2}{c^2} K_{\perp} - k_{\parallel}^2 + \frac{\omega^2}{c^2} K_x\right)\left(\frac{\omega^2}{c^2} K_{\perp} - k_{\parallel}^2 - \frac{\omega^2}{c^2} K_x\right)}{\frac{\omega^2}{c^2} K_{\perp} - k_{\parallel}^2} = \frac{CB}{A} \ . \tag{9}$$

For an axially symmetric, straight cylindrical tokamak, wave propagation proceeds at approximately constant $k_{\parallel}$ [11], and $k_{\perp}$ adjusts to satisfy the dispersion relation according to (9). Figure 1(a) shows the dependence of $k_{\perp}^2$ on $k_{\parallel}^2$ from (9) for a single-species plasma and fixed frequency ω. Figure 1(b) shows the dependence of ω on $k_{\parallel}$ for fixed $k_{\perp}^2$. In (9), resonance ($k_{\perp} \to \infty$) occurs when

$$A = \frac{\omega^2}{c^2} K_{\perp} - k_{\parallel}^2 = 0 \text{ (resonance)} \ . \tag{10}$$

Likewise, cutoff ($k_{\perp} = 0$) occurs when

$$B = \frac{\omega^2}{c^2}(K_{\perp} - K_x) - k_{\parallel}^2 = 0 \text{ (slow-wave cutoff)} \ , \tag{11}$$

$$C = \frac{\omega^2}{c^2}(K_{\perp} + K_x) - k_{\parallel}^2 = 0 \text{ (fast-wave cutoff)} \ . \tag{12}$$

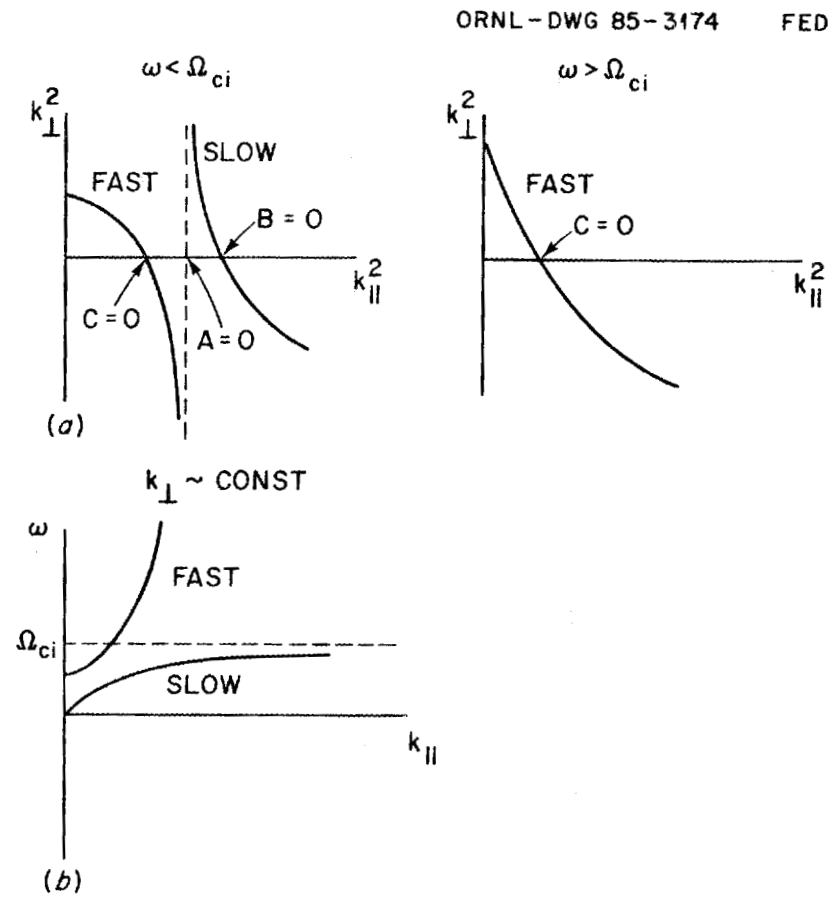

Fig. 1. Local dispersion relation for (a) fixed frequency and (b) fixed $k_\perp^2$.

The resonance $A = 0$ is called the "perpendicular ion cyclotron resonance" for a single-ion-species plasma and the "two-ion hybrid resonance" for a two-ion-species plasma. For a single ion species, $A = 0$ is only possible for $\omega < \Omega_{ci}$. The cutoff $C = 0$ is called the fast-wave cutoff and occurs for all values of ω. When $k_{\parallel}^2$ exceeds the cutoff value $\frac{\omega^2}{c^2}(K_{\perp} \pm K_x)$, the wave is evanescent, that is, $k_{\perp}^2 < 0$.

For a tokamak with toroidal and poloidal symmetry, $E \propto \exp i(m\theta + k_z z - \omega t)$, where $k_z = n/R_T$ and $k_\theta = m/r$. Defining $\lambda = (R_T/r)(B_\theta/B_z)$ and $b_z = B_z/B$, we have

$$k_{\parallel} = \vec{k} \cdot \frac{\vec{B}}{B} = b_z\left(k_z + m\,\frac{\lambda}{R_T}\right) .$$

3. DIELECTRIC TENSOR REPRESENTATION

Equation (5) for the dielectric tensor $\overleftrightarrow{K}$ is written in the coordinate system with the unperturbed magnetic field $\vec{B}_0$ in the z direction. For tokamak, mirror, and stellarator geometries this will not usually be the case. We therefore choose a right-handed, orthogonal coordinate system with unit vectors

$$\begin{aligned} \hat{\delta}_1 &= \nabla\psi/|\nabla\psi| \equiv \nabla\hat{\psi} , \\ \hat{\delta}_2 &= \hat{b} \times \nabla\hat{\psi} , \\ \hat{\delta}_3 &= \vec{B}_0/|B_0| = \hat{b} , \end{aligned} \tag{13}$$

where ψ is the flux function that defines a flux surface with $\hat{b} \cdot \nabla\hat{\psi} = 0$. We may then formally decompose the dielectric tensor $\overleftrightarrow{K}$ into its

components with the unit tensors $\hat{\delta}_1\hat{\delta}_1$, $\hat{\delta}_1,\hat{\delta}_2$, ..., which are dyadic products of the unit vectors. Thus (5) becomes

$$\overleftrightarrow{K} = K_\perp(\hat{\delta}_1\hat{\delta}_1 + \hat{\delta}_2\hat{\delta}_2) + iK_x(\hat{\delta}_2\hat{\delta}_1 - \hat{\delta}_1\hat{\delta}_2) + K_\perp(\hat{\delta}_3\hat{\delta}_3)$$

or

$$\overleftrightarrow{K} = K_\perp\left(\nabla\hat{\psi}\nabla\hat{\psi} + \hat{b} \times \nabla\hat{\psi}\ \hat{b} \times \nabla\hat{\psi}\right) + iK_x\left(\hat{b} \times \nabla\hat{\psi}\ \nabla\hat{\psi} - \nabla\hat{\psi}\ \hat{b} \times \nabla\hat{\psi}\right) + K_\parallel\left(\hat{b}\hat{b}\right) . \quad (14)$$

The components of $\overleftrightarrow{K}$ in the directions of $\hat{\delta}_1$, $\hat{\delta}_2$, and $\hat{\delta}_3$ are then

$$\nabla\hat{\psi} \cdot \overleftrightarrow{K} = K_\perp\nabla\hat{\psi} - iK_x\hat{b} \times \nabla\hat{\psi} ,$$

$$\hat{b} \times \nabla\hat{\psi} \cdot \overleftrightarrow{K} = K_\perp\hat{b} \times \nabla\hat{\psi} + iK_x\nabla\hat{\psi} ,$$

$$\hat{b} \cdot \overleftrightarrow{K} = K_\parallel\hat{b} ,$$

so that $\overleftrightarrow{K} \cdot \vec{E}$ becomes

$$\begin{aligned}\overleftrightarrow{K} \cdot \vec{E} = &\left(K_\perp\nabla\hat{\psi} \cdot \vec{E} - iK_x\ \hat{b} \times \nabla\hat{\psi} \cdot \vec{E}\right)\nabla\hat{\psi} \\ &+ \left(K_\perp\hat{b} \times \nabla\hat{\psi} \cdot \vec{E} + iK_x\nabla\hat{\psi} \cdot \vec{E}\right)\hat{b} \times \nabla\hat{\psi} + (K_\parallel\hat{b} \cdot \vec{E})\hat{b} . \quad (15)\end{aligned}$$

Likewise, from (5)

$$\overleftrightarrow{\sigma} \equiv \begin{pmatrix} \sigma_\perp & \sigma_x & 0 \\ -\sigma_x & \sigma_\perp & 0 \\ 0 & 0 & \sigma_\parallel \end{pmatrix} = -i\omega\varepsilon_0(\overleftrightarrow{K} - \overleftrightarrow{I}) = -i\omega\varepsilon_0 \begin{pmatrix} K_\perp - 1 & -iK_x & 0 \\ iK_x & K_\perp - 1 & 0 \\ 0 & 0 & K_\parallel \end{pmatrix} \quad (16)$$

so that $\overleftrightarrow{\sigma} \cdot \vec{E}$ can be written as

$$\overleftrightarrow{\sigma} \cdot \vec{E} = \left(\sigma_\perp \nabla\hat{\psi} \cdot \vec{E} + \sigma_x \hat{b} \times \nabla\hat{\psi} \cdot \vec{E}\right)\nabla\hat{\psi}$$
$$+ (\sigma_\perp \hat{b} \times \nabla\hat{\psi} \cdot \vec{E} - \sigma_x \nabla\hat{\psi} \cdot \vec{E})\hat{b} \times \nabla\hat{\psi} + (\sigma_\parallel \hat{b} \cdot \vec{E})\hat{b} \ . \tag{17}$$

4. THE STRAIGHT TOKAMAK WITH POLOIDAL FIELD

We consider a straight tokamak magnetic field in cylindrical coordinates r, θ, z,

$$\vec{B}_0 = B^0_\theta(r)\hat{\theta} + B^0_z(r,\theta)\vec{z} \ ,$$

with

$$B^0_z(r,\theta) = \frac{B_0}{1 + \frac{r}{R_T}\cos\theta} \tag{18}$$

$$B^0_\theta(r) = \lambda_0 B_0 \frac{r}{R_T} \begin{cases} 1 + \frac{c}{2}\frac{r^2}{a^2} + \frac{d}{3}\frac{r^4}{a^4} \ , & r \le a \\ \frac{a^2}{r^2}\left(1 + \frac{c}{2} + \frac{d}{3}\right) \ , & r > a \end{cases} \tag{19}$$

where c = -2.0, d = 1.0, a is the plasma radius, R_T is the major radius, and λ_0 is the rotational transform at r = 0 normalized to 2π. The rotational transform at radius r is

$$\lambda \equiv \frac{B_\theta^0}{B_z^0}\frac{R_T}{r} = \lambda_0\left(1 + \frac{r}{R_T}\cos\theta\right)\begin{cases} 1 + \frac{c}{2}\frac{r^2}{a^2} + \frac{d}{3}\frac{r^4}{a^4}, & r \le a \\ \frac{a^2}{r^2}\left(1 + \frac{c}{2} + \frac{d}{3}\right), & r > a \end{cases} . \tag{20}$$

Note that from $\vec{J} = \nabla \times \vec{H}$, $B_\theta^0(r)$ in (19) corresponds to a current density in the z direction,

$$J_z(r) = \frac{1}{\mu_0 r}\frac{\partial(rB_\theta^0)}{\partial r} = \frac{2B_0\lambda_0}{\mu_0 R_T}\begin{cases} 1 + c\frac{r^2}{a^2} + d\frac{r^4}{a^4}, & r \le a \\ 0, & r > a \end{cases} \tag{21}$$

For consistency we take the density profile n(r) proportional to (21).

Kovrizhnykh and Moroz [8] suggest that a finite gradient in $|B|$ along the magnetic field lines at resonance is important for direct ion cyclotron heating at the fundamental resonance. In cylindrical coordinates,

$$\vec{B}\cdot\nabla B = B_r\frac{\partial B}{\partial r} + B_\theta\frac{1}{r}\frac{\partial B}{\partial\theta} + B_z\frac{\partial B}{\partial z} .$$

For our assumed tokamak magnetic field in (18) and (19), $B_r = 0$ and $B^2 = B_\theta^2(r) + B_z^2(r,\theta)$. Thus,

$$\vec{B}\cdot\nabla B = B_\theta\frac{1}{r}\left(\frac{B_z}{B}\frac{\partial B_z}{\partial\theta}\right) = \lambda_0\frac{y}{R_T^2}\frac{B_z^3}{B}\left(1 + \frac{c}{2}\frac{r^2}{b^2} + \frac{d}{3}\frac{r^4}{b^4}\right) , \tag{22}$$

where $y = r\sin\theta$.

4.1 WAVE EQUATION FOR THE TOKAMAK

For straight tokamak geometry in cylindrical (r,θ,z) coordinates the flux function ψ can be chosen to be r. Then the three unit vectors in (13) are

$$\begin{aligned}
\hat{\delta}_1 &= \nabla\hat{\psi} = \hat{r} \ , \\
\hat{\delta}_2 &= \hat{b} \times \nabla\hat{\psi} = b_z\hat{\theta} - b_\theta\hat{z} \ , \\
\hat{\delta}_3 &= \hat{b} = b_\theta\hat{\theta} + b_z\hat{z} \ .
\end{aligned} \tag{23}$$

For this case (15) gives

$$\begin{aligned}
\overleftrightarrow{K} \cdot \vec{E} = &\left[K_\perp E_r - iK_x\left(b_z E_\theta - b_\theta E_z\right)\right]\hat{r} \\
&+ \left[K_\perp(b_z E_\theta - b_\theta E_z) + iK_x E_r\right](b_z\hat{\theta} - b_\theta\hat{z}) \\
&+ K_\parallel\left(b_\theta E_\theta + b_z E_z\right)\left(b_\theta\hat{\theta} + b_z\hat{z}\right) \ .
\end{aligned} \tag{24}$$

For ICRF frequencies ($\omega \sim \Omega_{ci}$) we make the assumption that the component of the wave electric field parallel to $\vec{B}_0$ is zero. The reasoning behind this assumption can be found in the relative magnitudes of the three components of the dielectric tensor. For $\omega \sim \Omega_{ci}$, (6) gives

$$\begin{aligned}
K_\perp &\sim \frac{-\omega_{pi}^2}{\omega^2 - \Omega_{ci}^2} \sim 0\left(\frac{\omega_{pi}^2}{\Omega_{ci}^2}\right) \ , \\
K_x &\sim -\frac{\omega}{\Omega_{ci}} K_\perp \sim 0\left(\frac{\omega_{pi}^2}{\Omega_{ci}^2}\right) \ ,
\end{aligned} \tag{25}$$

$$K_{\parallel} \sim O\left(\frac{\omega_{pe}^2}{\Omega_{ci}^2}\right) \sim O\left(\frac{\omega_{pi}^2}{\Omega_{ci}^2}\frac{m_i}{m_e}\right) .$$

Thus $K_{\parallel}$ is larger than $K_{\perp}$ and K_x by the ratio m_i/m_e, and, from the parallel component of the wave equation, $(\overleftrightarrow{K} \cdot \vec{E})_{\parallel} = K_{\parallel}E_{\parallel} \sim O(K_{\perp}E_{\perp})$,

$$E_{\parallel} = \hat{b} \cdot \vec{E} = O\left(\frac{m_e}{m_i}\right)E_{\perp} . \tag{26}$$

Physically, the high conductivity of the plasma along field lines shorts out the parallel electric fields on the time scale of the wave, $\Delta t \sim 2\pi/\Omega_{ci}$. Making the zero electron mass assumption in (26) with $\hat{b} = b_{\theta}\hat{\theta} + b_z\hat{z}$ gives

$$E_z \simeq \frac{-b_{\theta}}{b_z} E_{\theta} , \tag{27}$$

and (24) simplifies to

$$\overleftrightarrow{K} \cdot \vec{E} = \left(K_{\perp}E_r - i\,\frac{K_x}{b_z}\,E_{\theta}\right)\hat{r} + \left(K_{\perp}E_{\theta} + iK_x b_z E_r\right)\left(\hat{\theta} - \frac{b_{\theta}}{b_z}\,\hat{z}\right) . \tag{28}$$

In cylindrical coordinates, the curl operator is

$$\nabla \times \vec{E} = \left(\frac{1}{r}\frac{\partial E_z}{\partial \theta} - \frac{\partial E_{\theta}}{\partial z}\right)\hat{r} + \left(\frac{\partial E_r}{\partial z} - \frac{\partial E_z}{\partial r}\right)\hat{\theta} + \frac{1}{r}\left(\frac{\partial r E_{\theta}}{\partial r} - \frac{\partial E_r}{\partial \theta}\right)\hat{z} ,$$

and thus the components of $\nabla \times \nabla \times \vec{E}$ are

$$\left[\nabla \times \nabla \times \vec{E}\right]_r = \frac{1}{r}\frac{\partial}{\partial\theta}\left[\frac{1}{r}\frac{\partial rE_\theta}{\partial r} - \frac{1}{r}\frac{\partial E_r}{\partial\theta}\right] - \frac{\partial}{\partial z}\left[\frac{\partial E_r}{\partial z} - \frac{\partial E_z}{\partial r}\right] ,$$

$$\left[\nabla \times \nabla \times \vec{E}\right]_\theta = \frac{\partial}{\partial z}\left[\frac{1}{r}\frac{\partial E_z}{\partial\theta} - \frac{\partial E_\theta}{\partial z}\right] - \frac{\partial}{\partial r}\left[\frac{1}{r}\frac{\partial rE_\theta}{\partial r} - \frac{1}{r}\frac{\partial E_r}{\partial\theta}\right] ,$$

$$\left[\nabla \times \nabla \times \vec{E}\right]_z = \frac{1}{r}\frac{\partial}{\partial r} r\left[\frac{\partial E_r}{\partial z} - \frac{\partial E_z}{\partial r}\right] - \frac{1}{r}\frac{\partial}{\partial\theta}\left[\frac{1}{r}\frac{\partial E_z}{\partial\theta} - \frac{\partial E_\theta}{\partial z}\right] .$$

We now write (7) in cylindrical coordinates,

$$\begin{aligned}
&-\frac{1}{r}\frac{\partial}{\partial\theta}\left(\frac{1}{r}\frac{\partial}{\partial r} rE_\theta - \frac{1}{r}\frac{\partial E_r}{\partial\theta}\right) + \frac{\partial}{\partial z}\left[\frac{\partial E_r}{\partial z} + \frac{\partial}{\partial r}\left(\frac{b_\theta}{b_z} E_\theta\right)\right] + \frac{\omega^2}{c^2}\left(\overleftrightarrow{K}\cdot\vec{E}\right)_r \\
&\qquad = -i\omega\mu_0 J_r , \\
&\frac{\partial}{\partial z}\left[\frac{1}{r}\frac{\partial}{\partial\theta}\left(\frac{b_\theta}{b_z} E_\theta\right) + \frac{\partial E_\theta}{\partial z}\right] + \frac{\partial}{\partial r}\left(\frac{1}{r}\frac{\partial rE_\theta}{\partial r} - \frac{1}{r}\frac{\partial E_r}{\partial\theta}\right) + \frac{\omega^2}{c^2}\left(\overleftrightarrow{K}\cdot\vec{E}\right)_\theta \\
&\qquad = -i\omega\mu_0 J_\theta , \\
&-\frac{1}{r}\frac{\partial}{\partial r} r\left[\frac{\partial E_r}{\partial z} + \frac{\partial}{\partial r}\left(\frac{b_\theta}{b_z} E_\theta\right)\right] - \frac{1}{r}\frac{\partial}{\partial\theta}\left[\frac{1}{r}\frac{\partial}{\partial\theta}\left(\frac{b_\theta}{b_z} E_\theta\right) + \frac{\partial E_\theta}{\partial z}\right] + \frac{\omega^2}{c^2}\left(\overleftrightarrow{K}\cdot\vec{E}\right)_z \\
&\qquad = -i\omega\mu_0 J_z ,
\end{aligned} \tag{29}$$

where we have used (27) to eliminate E_z. We now Fourier analyze in the z direction with

$$\vec{E}(r,\theta,z) = \sum_{k_z} \vec{E}_{k_z}(r,\theta)\, e^{ik_z z} , \tag{30}$$

$$\vec{J}(r,\theta,z) = \sum_{k_z} J_{k_z}(r,\theta)\, e^{ik_z z} \tag{31}$$

and (29) becomes (dropping the subscript k_z from $\vec{E}$ for brevity)

$$- \frac{1}{r} \frac{\partial}{\partial\theta}\left(\frac{1}{r} \frac{\partial rE_\theta}{\partial r} - \frac{1}{r} \frac{\partial E_r}{\partial\theta}\right) + ik_z\left[ik_zE_r + \frac{\partial}{\partial r}\left(\frac{b_\theta}{b_z} E_\theta\right)\right] + \frac{\omega^2}{c^2} \left(\overleftrightarrow{K} \cdot \vec{E}\right)_r$$

$$= -i\omega\mu_0 J_{r,k_z} ,$$

$$ik_z\left[\frac{1}{r} \frac{\partial}{\partial\theta}\left(\frac{b_\theta}{b_z} E_\theta\right) + ik_zE_\theta\right] + \frac{\partial}{\partial r}\left(\frac{1}{r} \frac{\partial rE_\theta}{\partial r} - \frac{1}{r} \frac{\partial E_r}{\partial\theta}\right)$$

$$+ \frac{\omega^2}{c^2} \left[\left(\overleftrightarrow{K} \cdot \vec{E}\right)_\theta - \frac{b_\theta}{b_z}\left(\overleftrightarrow{K} \cdot \vec{E}\right)_z\right] - \frac{b_\theta}{b_z} \left\{-\frac{1}{r} \frac{\partial}{\partial r} r\left[ik_zE_r + \frac{\partial}{\partial r}\left(\frac{b_\theta}{b_z} E_\theta\right)\right]\right.$$

$$\left. - \frac{1}{r} \frac{\partial}{\partial\theta}\left[\frac{1}{r} \frac{\partial}{\partial\theta} \left(\frac{b_\theta}{b_z} E_\theta\right) + ik_zE_\theta\right]\right\} = -i\omega\mu_0 \left(J_{\theta,k_z} - \frac{b_\theta}{b_z} J_{z,k_z}\right) , \tag{32}$$

where we have combined the θ and z components to give the $\hat{\delta}_2 = \hat{b} \times \nabla\hat{\psi}$ component, perpendicular to both $\hat{b}$ and $\nabla\hat{\psi} = \hat{r}$.

Defining $u = rE_r$ and $v = rE_\theta$ and using (28), we can write the differential equations in (32) are

$$\frac{1}{r^2} \frac{\partial^2 u}{\partial\theta^2} - \frac{1}{r} \frac{\partial^2 v}{\partial r\partial\theta} + \left(\frac{\omega^2}{c^2} K_\perp - k_z^2\right)u - i \frac{\omega^2}{c^2} \frac{K_x}{b_z} v + \frac{ik_z}{R_T} r \frac{\partial\lambda v}{\partial r} = -i\omega\mu_0 rJ_{r,k_z} , \tag{33}$$

$$r\frac{\partial}{\partial r}\left(\frac{1}{r} \frac{\partial v}{\partial r}\right) - r \frac{\partial}{\partial r}\left(\frac{1}{r^2} \frac{\partial u}{\partial\theta}\right) + \left(\frac{\omega^2}{c^2} \frac{K_\perp}{b_z^2} - k_z^2\right)v + i \frac{\omega^2}{c^2} \frac{K_x}{b_z} u + \frac{ik_z}{R_T} \frac{\partial\lambda v}{\partial\theta}$$

$$+ i \frac{\lambda k_z}{R_T} \left(r \frac{\partial u}{\partial r} + \frac{\partial v}{\partial\theta}\right) + \frac{\lambda}{R_T^2} \left[r \frac{\partial}{\partial r}\left(r \frac{\partial\lambda v}{\partial r}\right) + \frac{\partial^2\lambda v}{\partial\theta^2}\right]$$

$$= -i\omega\mu_0 r\left(J_{\theta,k_z} - \frac{\lambda r}{R_T} J_{z,k_z}\right) . \tag{34}$$

In the limit that $\lambda = 0$, i.e., no poloidal magnetic field, (33) and (34) reduce to

$$\frac{1}{r^2}\frac{\partial^2 u}{\partial\theta^2} - \frac{1}{r}\frac{\partial^2 v}{\partial r\partial\theta} + \left(\frac{\omega^2}{c^2}K_\perp - k_z^2\right)u - i\frac{\omega^2}{c^2}K_x v = -i\omega\mu_0 r J_{r,k_z} ,$$

$$r\frac{\partial}{\partial r}\left(\frac{1}{r}\frac{\partial v}{\partial r}\right) - r\frac{\partial}{\partial r}\left(\frac{1}{r^2}\frac{\partial u}{\partial\theta}\right) + \left(\frac{\omega^2}{c^2}K_\perp - k_z^2\right)v + i\frac{\omega^2}{c^2}K_x u = -i\omega\mu_0 r J_{\theta,k_z} ,$$

which are the equations solved by Itoh et al. in ref. [1].

4.2 LOCAL ENERGY DEPOSITION AND ANTENNA IMPEDANCE IN THE TOKAMAK

The local energy deposition rate $\dot{W}(r,\theta)$ is the time average over a wave period of $\mathrm{Re}\,\vec{J}_{plasma} \cdot \mathrm{Re}\,\vec{E}$. Assuming $\vec{E}$ and $\vec{J}_{plasma}$ are proportional to $e^{-i\omega t}$ and performing the time average gives

$$\dot{W}(r,\theta) = \frac{1}{2}\,\mathrm{Re}\left(\vec{J}^{*}_{plasma} \cdot \vec{E}\right) = \frac{1}{2}\,\mathrm{Re}(\vec{E}^{*} \cdot \vec{J}_{plasma}) . \tag{35}$$

Now $\vec{J}_{plasma} = \overleftrightarrow{\sigma} \cdot \vec{E}$ and from (17) with $\nabla\hat{\psi} = \hat{r}$, $\hat{b} \times \nabla\hat{\psi} = b_z\hat{\theta} - b_\theta\hat{z}$, and $\hat{b} = b_\theta\hat{\theta} + b_z\hat{z}$, we have

$$\overleftrightarrow{\sigma} \cdot \vec{E} = \left[\sigma_\perp E_r + \sigma_x\left(b_z E_\theta - b_\theta E_z\right)\right]\hat{r} + \left[\sigma_\perp\left(b_z E_\theta - b_\theta E_z\right) - \sigma_x E_r\right]\left(b_z\hat{\theta} - b_\theta\hat{z}\right)$$

$$+ \sigma_\parallel\left(b_\theta E_\theta + b_z E_z\right)\left(b_\theta\hat{\theta} + b_z\hat{z}\right) .$$

Noting that

$$E_{\parallel} = \vec{E} \cdot \hat{b} = b_{\Theta}E_{\Theta} + b_z E_z = 0 \ ,$$

$$E_{\chi} = \vec{E} \cdot \hat{b} \times \nabla\hat{\psi} = b_z E_{\Theta} - b_{\Theta}E_z = \frac{E_{\Theta}}{b_z} \ , \tag{36}$$

we find

$$\vec{E}^* \cdot \vec{J}_{plasma} = \vec{E}^* \cdot \overleftrightarrow{\sigma} \cdot \vec{E} = \sigma_{\perp}|E_{\perp}|^2 + \sigma_{\parallel}|E_{\parallel}|^2 + \sigma_x 2i \ \mathrm{Im}\ E_r^* E_{\chi} \ , \tag{37}$$

where

$$|E_{\perp}|^2 = E_r^* E_r + E_{\chi}^* E_{\chi} \ .$$

Finally, substituting into (35) and using (16) gives

$$\dot{W}(r,\Theta) = \frac{1}{2}\ \omega\varepsilon_0\left[\mathrm{Im}(K_{\perp} - 1)|E_{\perp}|^2 + 2\ \mathrm{Im}(K_x)\mathrm{Im}(E_r^* E_{\chi}) + \mathrm{Im}\ K_{\parallel}|E_{\parallel}|^2\right] \ , \tag{38}$$

where for $E_{\parallel} = 0$ and $K_{\parallel} = \infty$, the third term is zero.

If we define E_+ and E_- to be the left- and right-hand circularly polarized waves, respectively,

$$E_+ = E_r + iE_{\chi} \ ,$$
$$E_- = E_r - iE_{\chi} \ , \tag{39}$$

then the transformation $\overleftrightarrow{T}$ can be defined such that $\vec{E}' = \overleftrightarrow{T} \cdot \vec{E}$, where $E' = (E_+, E_-, E_{\parallel})$, $\vec{E} = (E_r, E_{\chi}, E_{\parallel})$, and

$$\overleftrightarrow{T} = \begin{pmatrix} 1 & i & 0 \\ 1 & -i & 0 \\ 0 & 0 & 1 \end{pmatrix}, \quad \overleftrightarrow{T}^{-1} = \frac{1}{2}\begin{pmatrix} 1 & 1 & 0 \\ -i & i & 0 \\ 0 & 0 & 2 \end{pmatrix}.$$

Applying this transformation to the conductivity tensor in (16) gives

$$J' = (\overleftrightarrow{T}\overleftrightarrow{\sigma}\overleftrightarrow{T}^{-1})\vec{E}' = \begin{pmatrix} \sigma_{++} & 0 & 0 \\ 0 & \sigma_{--} & 0 \\ 0 & 0 & \sigma_{\parallel} \end{pmatrix}\begin{pmatrix} E_+ \\ E_- \\ E_{\parallel} \end{pmatrix},$$

where $J' = (J^+, J^-, J_{\parallel})$ and

$$\sigma_{++} = \sigma_\perp - i\sigma_x = -i\omega\varepsilon_0(L - 1) ,$$

$$\sigma_{--} = \sigma_\perp + i\sigma_x = -i\omega\varepsilon_0(R - 1) , \tag{40}$$

where we have defined [10] $L \equiv K_\perp - K_x$ and $R \equiv K_\perp + K_x$. Using (40), (35) gives

$$\dot{W}(r,\theta) = \frac{1}{4}\left[\mathrm{Re}(\sigma_{++})|E_+|^2 + \mathrm{Re}(\sigma_{--})|E_-|^2 + 2\ \mathrm{Re}(\sigma_{\parallel})|E_{\parallel}|^2\right] , \tag{41}$$

which is equivalent to (38).

From (40) and (25) we note that

$$\frac{\sigma_{++}}{\sigma_{--}} = \frac{L - 1}{R - 1} = \frac{K_\perp(1 + \omega/\Omega_{ci}) - 1}{K_\perp(1 - \omega/\Omega_{ci}) - 1} .$$

If, in addition, the density is high enough that $K_\perp \gg 1$, then

$$\frac{\sigma_{++}}{\sigma_{--}} \simeq \frac{\Omega_{ci} + \omega}{\Omega_{ci} - \omega} \gg 1 \quad (\text{for } \Omega_{ci} \geq \omega) .$$

Thus, for high densities ($K_\perp \gg 1$) with $\Omega_{ci} \geq \omega$, one expects the right-hand polarized component E_- to penetrate the plasma significantly more easily than the left-hand polarized component E_+. For low densities ($K_\perp \lesssim 1$), one expects both polarizations to penetrate equally well.

Integrating $\dot{W}(r,\theta)$ over r and θ gives the power absorbed per unit length for one toroidal eigenmode corresponding to one k_z:

$$P_{abs}(k_z,\omega) = \int r\, dr \int d\theta\, \dot{W}(r,\theta) . \tag{42}$$

The total power absorbed by the plasma P_{tot} is found by summing (42) over all k_z and integrating around the toroidal circumference $2\pi R_T$. Then dividing by $|I|^2/2$ gives the plasma loading resistance $\hat{R}(\omega)$,

$$\hat{R}(\omega) = \frac{2P_{tot}}{|I|^2} = \frac{2}{|I|^2}\, 2\pi R_T \sum_{k_z} P_{abs}(k_z,\omega) , \tag{43}$$

where I is the antenna current corresponding to $\vec{J}_{ext}$ in (7). Likewise, the power circulating in the antenna per unit length $P_c(k_z,\omega)$ is found from $\frac{1}{2}J^*_{ext} \cdot \vec{E} = \frac{1}{2}(J^*_r E_r + J^*_\theta E_\theta + J^*_z E_z)$, so that

$$P_c(k_z,\omega) = \frac{1}{2} \int r\, dr \int d\theta \left[J^*_r E_r + \left(J^*_\theta - \frac{b_\theta}{b_z} J^*_z\right) E_\theta\right] . \tag{44}$$

The antenna impedance $Z(\omega)$ is found by summing (44) over k_z, integrating around the toroidal circumference, and dividing by $\frac{1}{2}|I|^2$:

$$Z(\omega) = \frac{2P_c}{|I|^2} = \frac{2}{|I|^2}\, 2\pi R_T \sum_{k_z} P_c(k_z,\omega) \ . \tag{45}$$

The real part of the antenna impedance Re(Z) is the antenna resistance and must equal the plasma loading resistance $\hat{R}(\omega)$ for a lossless system. $\hat{R}(\omega)$ corresponds to the real power absorbed by the plasma in (42).

The imaginary part of the antenna impedance Im(Z) is the antenna reactance and corresponds to power recirculated between the antenna and the plasma because $\vec{J}$ and $\vec{E}$ are out of phase.

4.3 ANTENNA CURRENT FOR THE TOKAMAK

We assume a Gaussian current distribution [1] in the toroidal (z) direction with width L_T:

$$\vec{J}_{(r,\theta,z)} = \frac{I_0 f(\theta)}{\sqrt{\pi} L_T}\, \delta(r - r_0)\left\{\exp(-z^2/L_T^2) + \exp\left[\frac{-(z - 2\pi R_T)^2}{L_T^2}\right] + \ldots\right\}\hat{\theta} \ . \tag{46}$$

Equation (46) has been normalized so that $\int dr \int dz\ \vec{J}_{(r,\theta,z)} = I_0 f(\theta)\hat{\theta}$ when $L_T \ll \pi R_T$ and can be represented by the Fourier sum

$$\vec{J}_{(r,\theta,z)} = \frac{I_0 f(\theta)}{2\pi R_T}\, \delta(r - r_0)\ \hat{\theta} \sum_{l=-\infty}^{\infty} \exp\left(-\frac{l^2 L_T^2}{4R_T^2} + \frac{ilz}{R_T}\right) , \tag{47}$$

where $k_z = 1/R_T$. Thus, $\vec{J}_{k_z}(r,\theta)$ in (31) is

$$\vec{J}_{k_z}(r,\theta) = \frac{\delta(r - r_0)}{2\pi R_T}\,\hat{\theta} I_0 f(\theta)\,\exp\left(-\frac{l^2 L_T^2}{4R_T^2}\right) . \tag{48}$$

In practice we solve (33) and (34) with $I_0 = 1$ A and $l = 0$, so that

$$\vec{J}_{k_z}(r,\theta) = \frac{\delta(r - r_0)}{2\pi R_T}\hat{\theta} f(\theta) , \tag{49}$$

and then include arbitrary L_T and I_0 when summing the two-dimensional (2-D) solutions that make up the Fourier expansion. This allows calculations for arbitrary antenna lengths (in z) and currents with just one set of toroidal eigenmodes. The function $f(\theta)$ gives the poloidal (θ) dependence of the antenna current. We take a periodic Gaussian [1]

$$f(\theta) = f_0 \sum_{n=-\infty}^{\infty} \exp\left[-\left(\frac{\theta - 2\pi n + \pi p}{\pi\Delta}\right)^2\right] , \tag{50}$$

where f_0 is chosen so that the maximum value of $f(\theta)$ is unity. For $p = 0$, $f(\theta)$ is maximum at $\theta = 0, 2\pi$, corresponding to low-field excitation. For $p = 1$, $f(\theta)$ is maximum at $\theta = \pi$, corresponding to high-field excitation. At these poloidal locations the normalization in (46) gives $\int dr \int dz\, \vec{J}(r,\theta,z) = I_0\hat{\theta}$. The parameter Δ controls the poloidal (θ) extent of the current as shown in Fig. 2. Note from the figure that $\Delta \geq 2.0$ approximates the $m = 0$ case, i.e., no poloidal dependence of the antenna current.

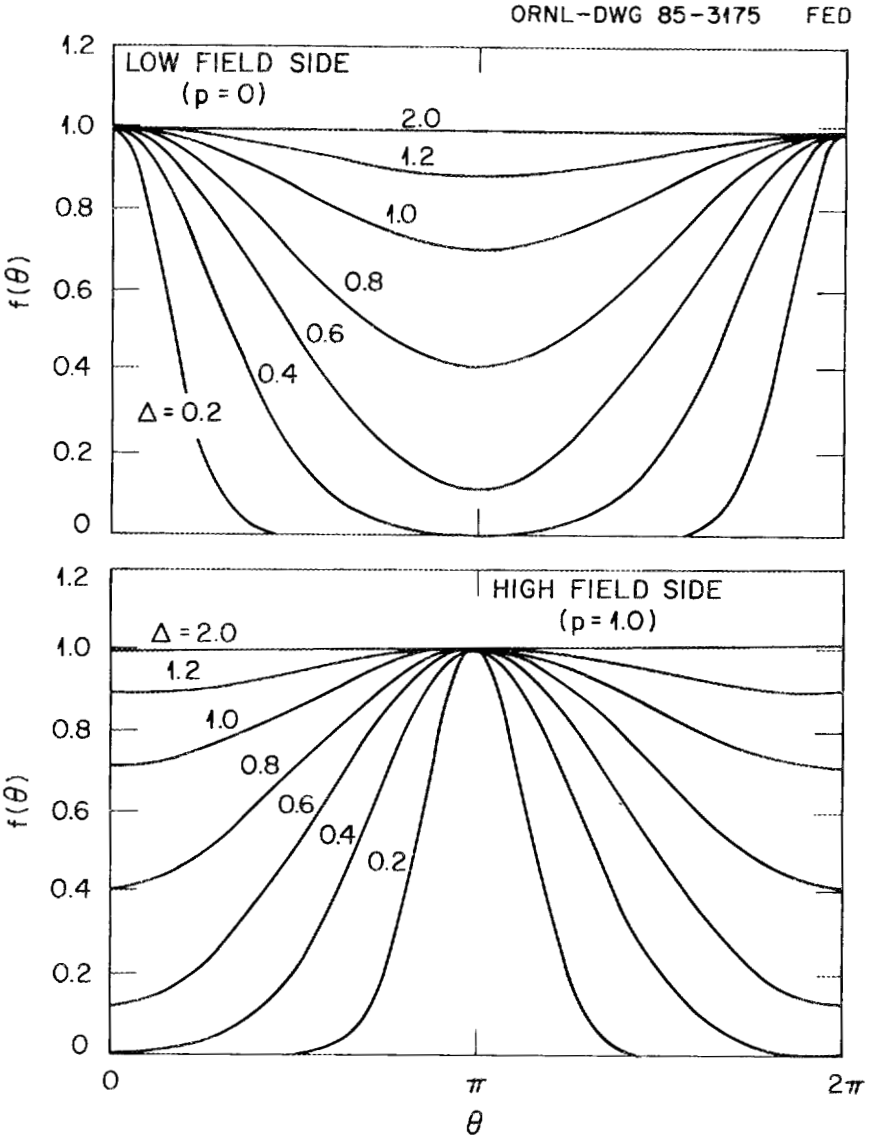

Fig. 2. Poloidal variation of the assumed antenna current.

5. NUMERICAL RESULTS FOR THE TOKAMAK

In this section we display numerical results for the tokamak with arbitrary rotational transform. Figure 3(a) shows schematically the geometry treated. A plasma of radius a_p is contained inside a cylindrical, perfectly conducting metal wall of radius a_{wall}. In general, there may be vacuum present in the region $a_p < r < a_{wall}$. The dashed line represents a current-carrying antenna of radius a_{ant}. The current in the antenna can be concentrated on the low-field side (right, $p = 0$), on the high-field side (left, $p = 1.0$), or at an arbitrary poloidal location and can have an arbitrary poloidal extent ($0 < \Delta \leq \infty$). Figure 3(b) shows the assumed profile (22) for the plasma current $J_z(r)$ and density $n(r)$ along with the corresponding poloidal magnetic field B_θ and rotational transform ι [see (19)-(21)].

5.1 TWO-ION HYBRID RESONANCE

Equations (33) and (34) are solved in this geometry using a finite difference mesh of 36 poloidal and 29 radial mesh points. For Figs. 4-11 we assume parameters typical of the proposed Tore Supra superconducting tokamak experiment. This is a large, high-density, high-magnetic-field experiment with

$$B_0 \sim 4.0 \text{ T} ,$$

$$R_T = 2.25 \text{ m} ,$$

$$a_{wall} = 0.90 \text{ m} ,$$

$$\left.\begin{array}{l} a_p = 0.70 \text{ m} \\ a_{ant} \sim 0.77 \text{ m} \end{array}\right\} \delta_1 = a_{ant} - a_p \sim 0.07 \text{ m} ,$$

ORNL-DWG 85-3176 FED

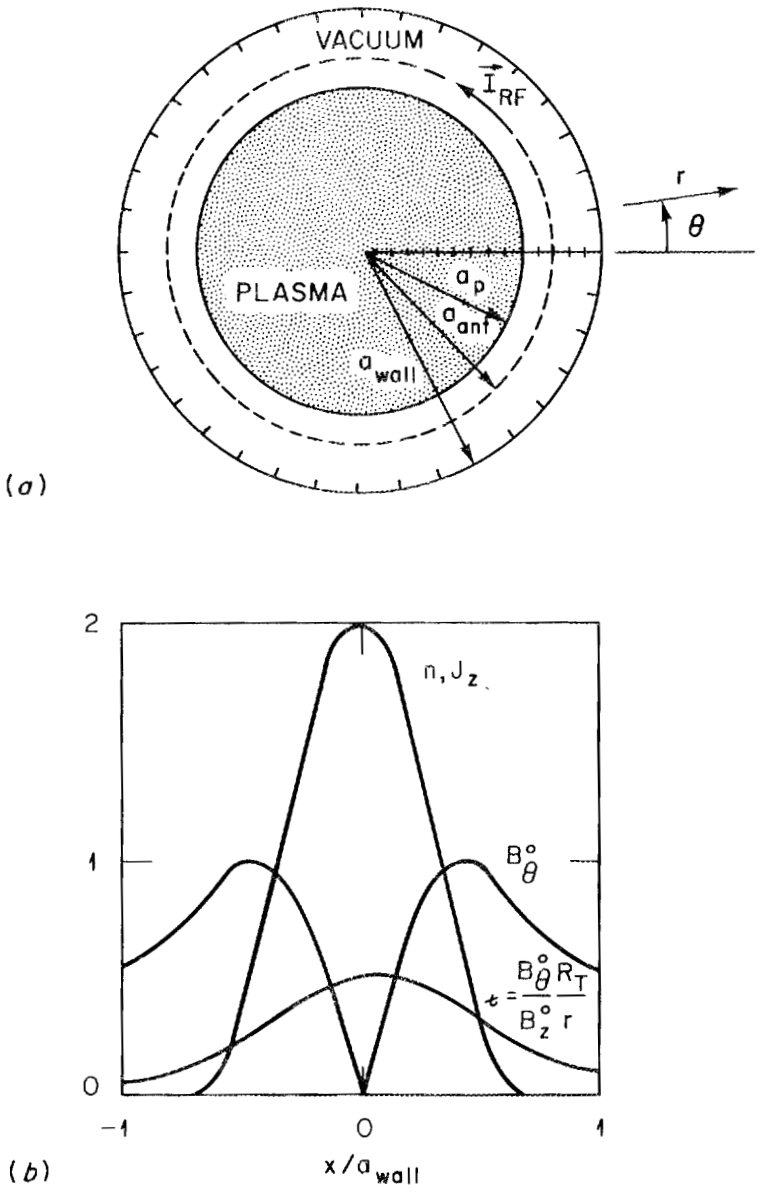

Fig. 3. (a) Tokamak geometry and (b) assumed profiles for density, current, and poloidal magnetic field.

$$\left.\begin{array}{l}\text{Majority density } n_{D_2^+} = 1 \times 10^{14}\ \text{cm}^{-3} \\ \text{Minority density } n_{H^+} = 1 \times 10^{13}\ \text{cm}^{-3}\end{array}\right\} \eta = \frac{n_{H^+}}{n_{D_2^+}} = 10\% \ ,$$

$I_{plasma} = 1.7 \times 10^6$ A $\rightarrow \lambda_0 \sim 1.0$,

f = 55 MHz .

This choice of frequency and density ratio puts the two-ion hybrid resonance just on the low-field side of the plasma center.

Figure 4 compares electric field contours for the l = 4 toroidal eigenmode and two different antenna geometries, both centered at $\Theta = 0$, i.e., the low-field side of the plasma. Only the real parts of the field are shown. The contours on the left [Fig. 4(a)] result from a compact antenna design with $\Delta = 0.1$, corresponding to a poloidal half-width at e^{-1} of maximum of $\Delta\Theta \sim 18^o$ or $\Delta s \sim 24$ cm, where s is the arc length along the antenna. Contours on the right [Fig. 4(b)] are for an approximate half-turn antenna with $\Delta = 0.4$, corresponding to a half-width $\Delta\Theta \sim 72^o$ or $\Delta s \sim 96$ cm. Note that for both antenna geometries, the fields tend to focus toward r = 0 and the contours of E_- penetrate the plasma more easily than those of E_+.

In Fig. 5, 81 toroidal eigenmode solutions (l = -40, ..., +40) as shown in Fig. 4 have been combined to give the complete three-dimensional (3-D) result for the compact antenna case in Fig. 4. For the solution shown, an antenna with $\pi R_T/L_T = 30$ has been assumed and corresponds to a toroidal half-width of about $L_T = 23.5$ cm. Results in Fig. 5 are plotted in a poloidal plane located at the midplane of the antenna in the toroidal direction. Results may also be plotted as in Figs. 6 and 7 in the r,z equatorial plane where $\Theta = 0,\pi$. The toroidal half-width of the antenna L_T is labeled explicitly here ($z = 0,2\pi R_T$ corresponds to the

ORNL-DWG 85-3177 FED

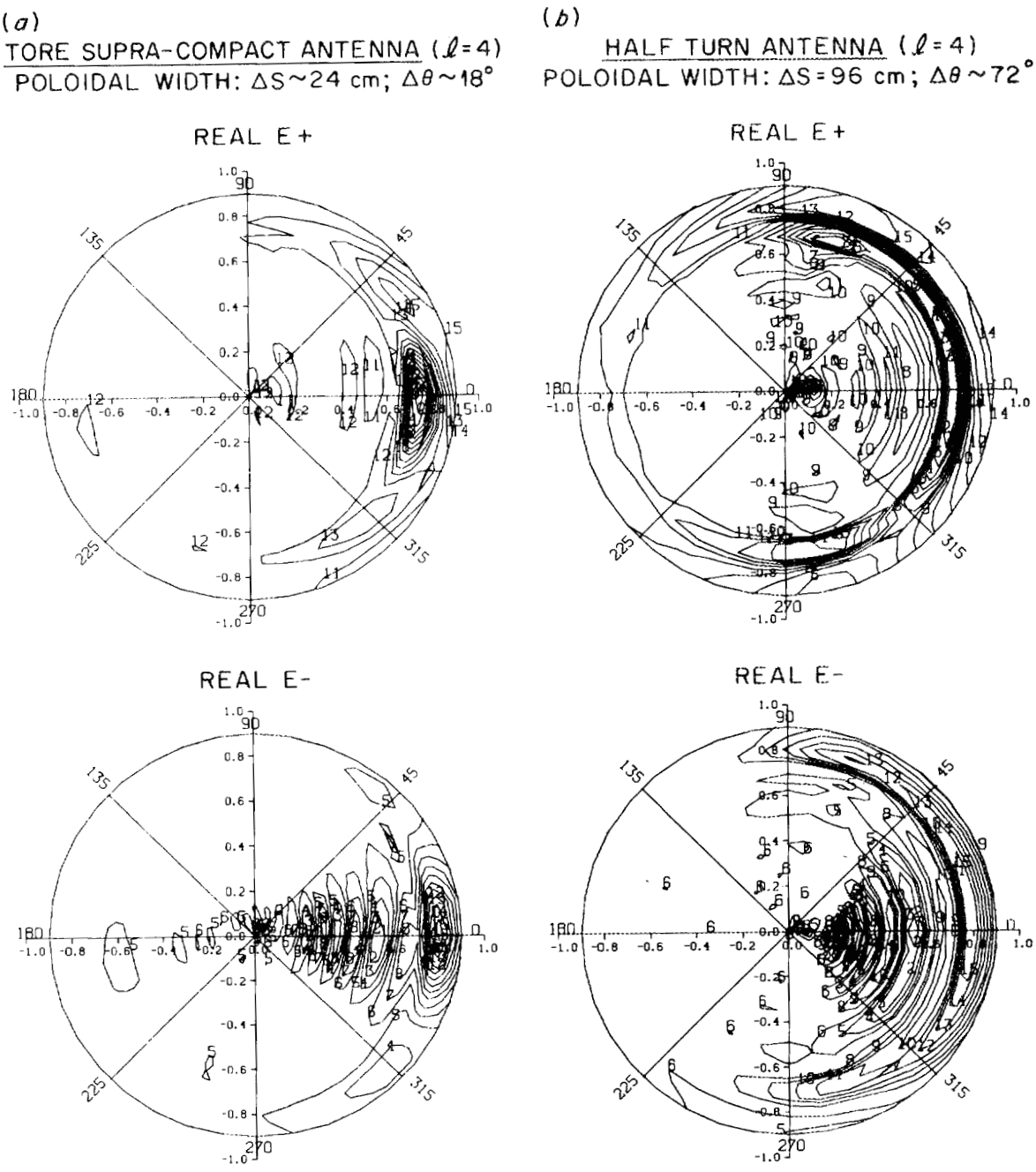

Fig. 4. Electric field contours for the l = 4 toroidal mode in the Tore Supra tokamak with (a) compact and (b) half-turn antennas on the low-field (right) side.

ORNL-DWG 85-3178 FED

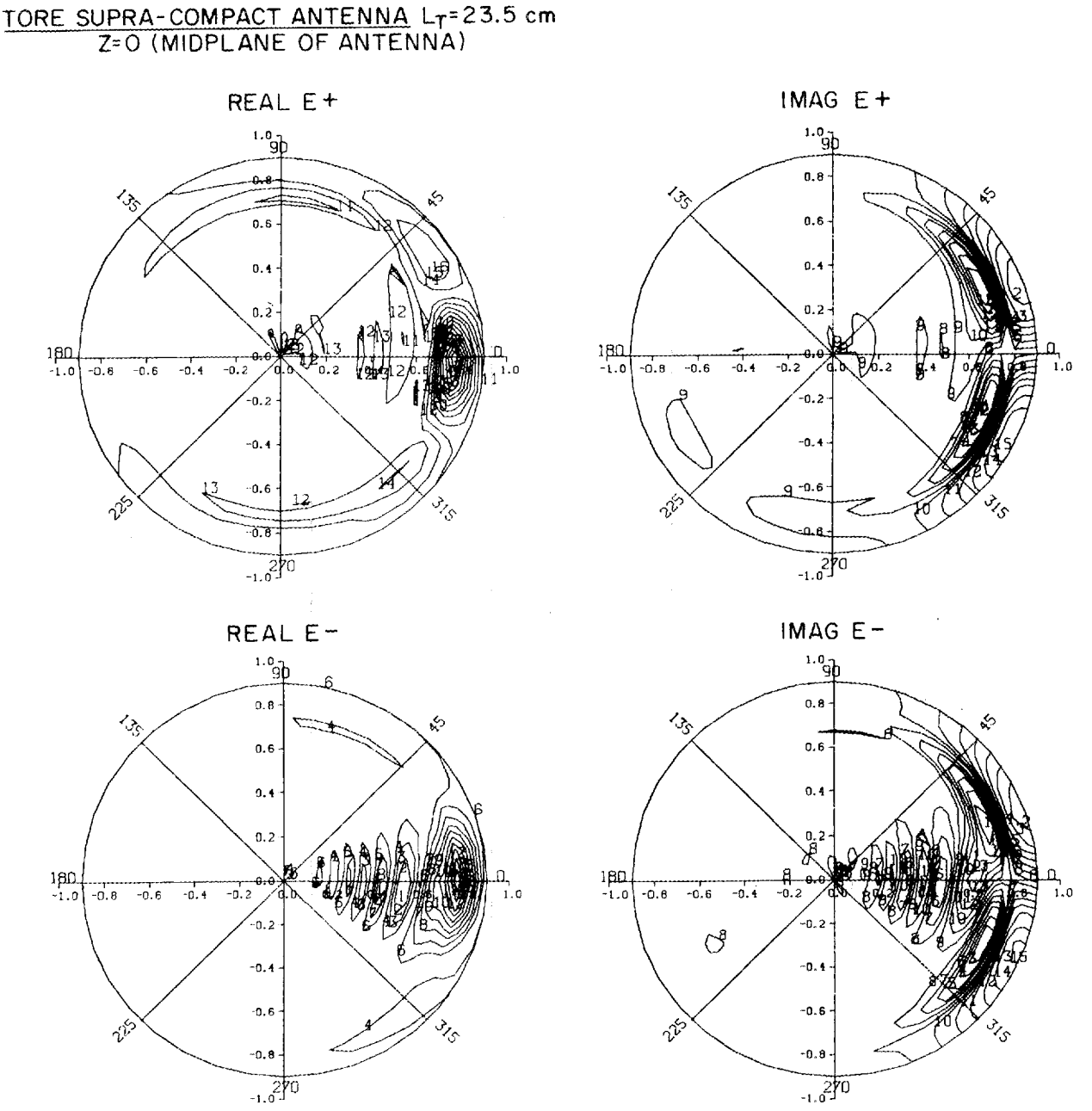

Fig. 5. r-θ contours of the 3-D electric field plotted in the midplane of the compact antenna with toroidal half-width L_T = 23.5 cm.

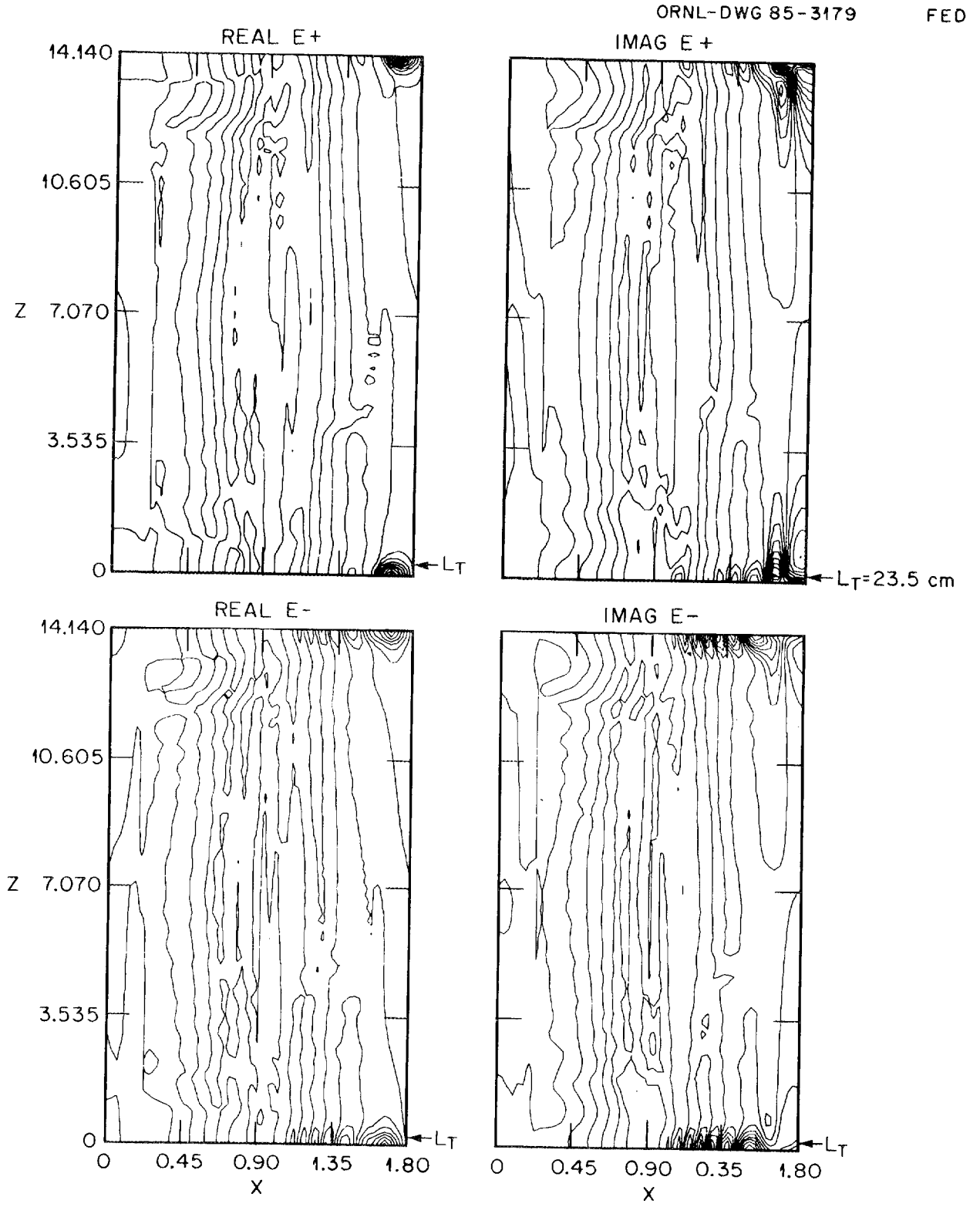

Fig. 6. r-z contours of the 3-D electric field in the equatorial plane ($\theta = 0,\pi$) for the case of Fig. 5.

ORNL-DWG 85-3180 FED

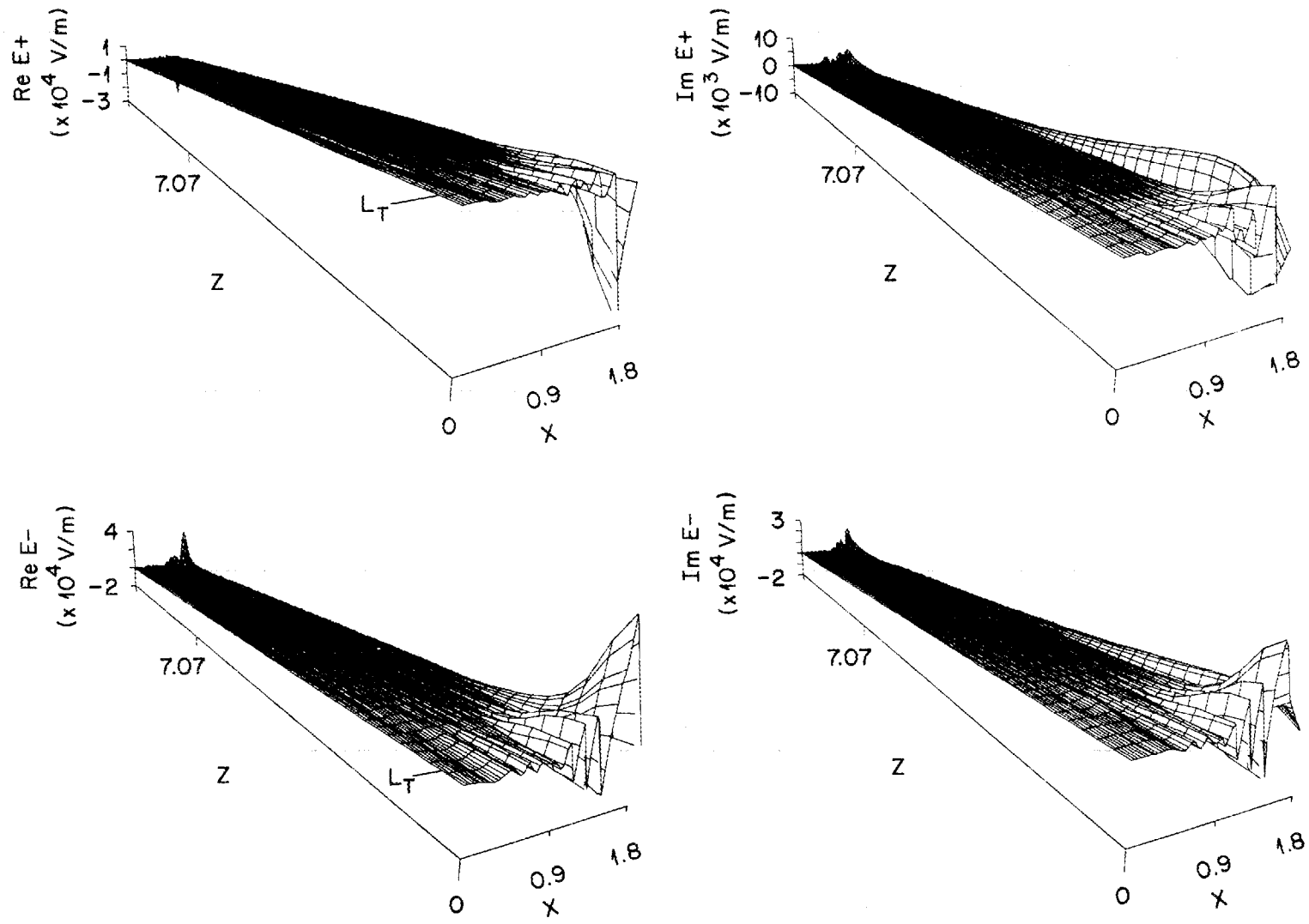

Fig. 7. 3-D contour plot of the result in Fig. 6.

antenna midplane). Note the penetration of the fields, especially E_-, on the low-field (right) side near the antenna location ($z = 0, 2\pi R_T$) in these figures.

For the case of no rotational transform ($\lambda = 0$), k_z enters (33), (34) only quadratically. In this case, $E_{-k_z}(r,\theta) = E_{+k_z}(r,\theta)$, so that only toroidal modes with $k_z \geq 0$ need be calculated explicitly. Furthermore, the Fourier sum in (30) gives

$$\vec{E}(r,\theta,z) = \sum_{k_z=1}^{\infty} 2E_{k_z}(r,\theta)\cos k_z z + E_0(r,\theta) ,$$

so the solutions are symmetric in z about the antenna midplane ($z = 0, 2\pi R_T$). However, for $\lambda \neq 0$, linear terms in k_z arise in (33),(34) and therefore $E_{k_z}(r,\theta) \neq E_{-k_z}(r,\theta)$. Thus, negative k_z's must be calculated explicitly. Since $\sin k_z z$ terms now also contribute to the Fourier sum in (30), symmetry in z about the antenna midplane is destroyed. Thus, we plot the complete toroidal range $0 < z \leq 2\pi R_T$ in Figs. 6 and 7.

Figures 5-7 assume a uniform background plasma of density $n = 10^{11}$ cm^{-3} in the region between the wall and plasma ($a_p < r < a_{wall}$). Figures 8-10 show the same case but with an ideal vacuum in the region surrounding the plasma. Note the presence of an $l = 2$ cavity mode in this vacuum region. Such modes are typically not observed in experiments [12]. Furthermore, they are undesirable because when real wall losses are included, the large electric fields near the wall around the entire torus lead to excessive absorption of wave energy and reduced efficiency [12]. On the other hand, when there is a low-density background plasma between the wall and the main plasma as in Figs. 5-7, the undesirable $l = 2$ vacuum mode is completely suppressed, and large electric fields occur only in the immediate vicinity of the antenna structure.

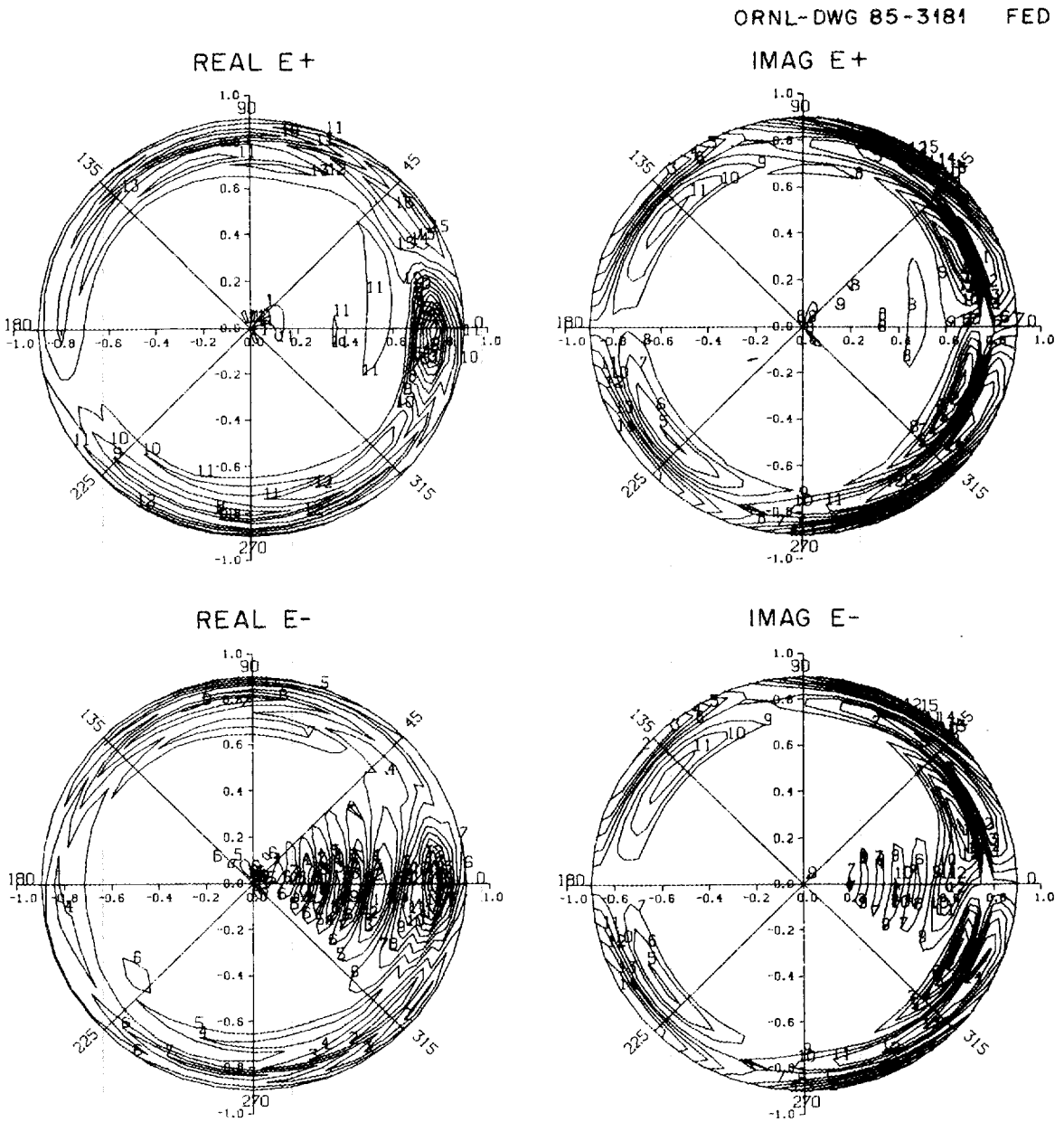

Fig. 8. The case of Fig. 5 with ideal vacuum surrounding the plasma.

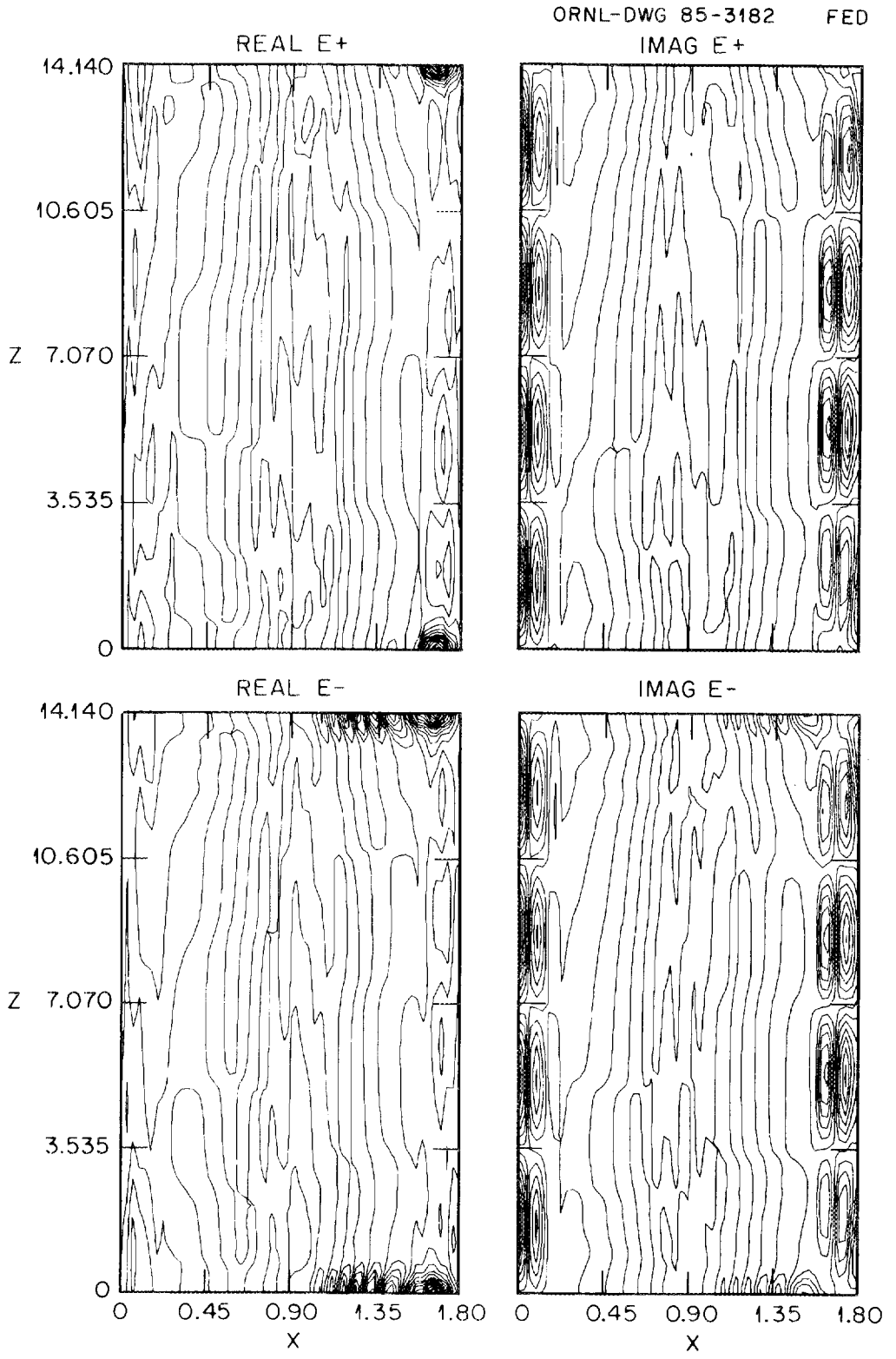

Fig. 9. The case of Fig. 6 with ideal vacuum surrounding the plasma.

ORNL-DWG 85-3183 FED

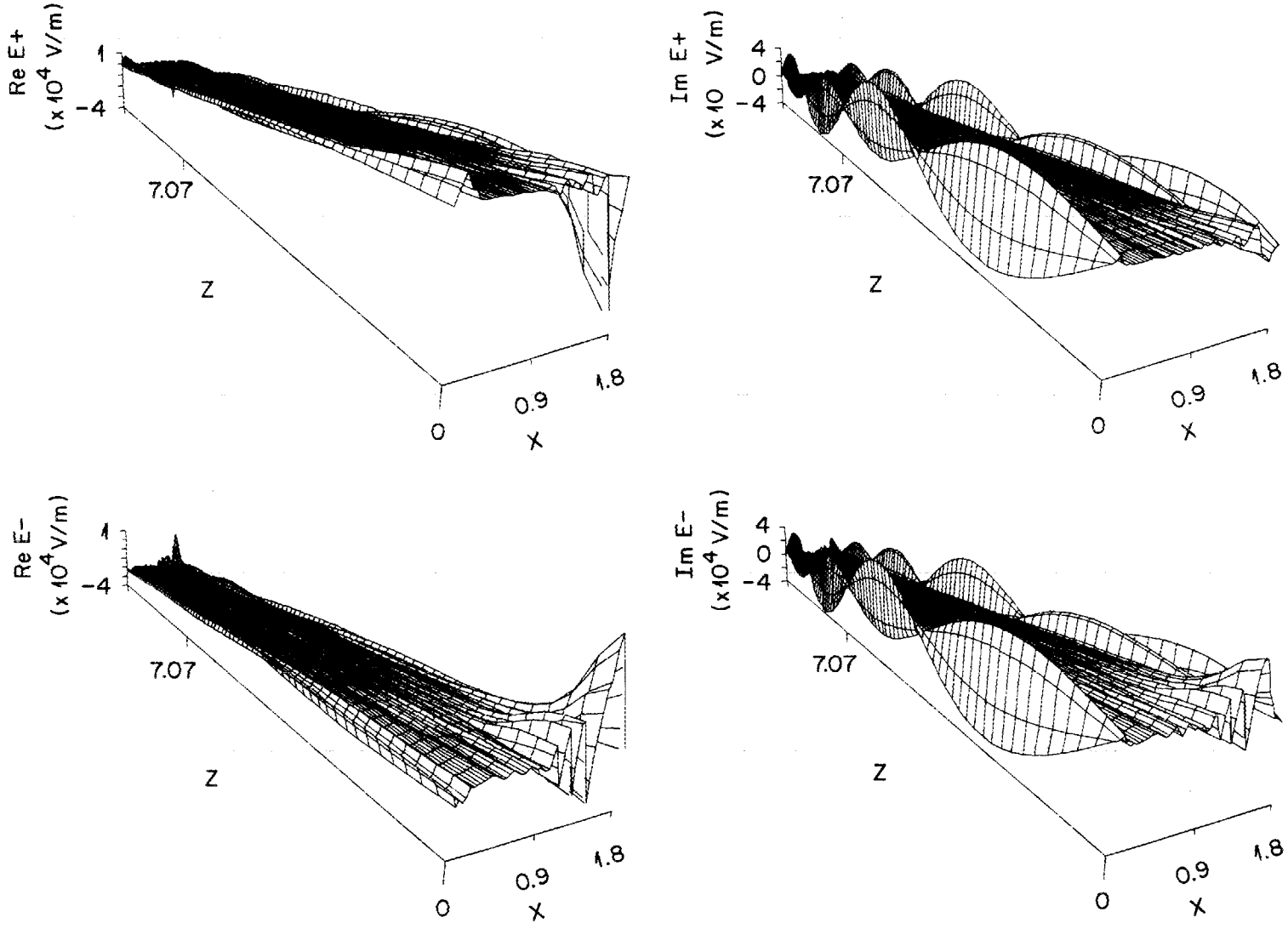

Fig. 10. The case of Fig. 7 with ideal vacuum surrounding the plasma.

Once the electric fields have been calculated, the energy absorption can be found from either (38) or (41) and the antenna impedance from (45). Figure 11 shows the local energy absorption for both the compact [Figure 11(a)] and half-turn [Fig. 11(b)] antenna geometries of Fig. 4. These are again 3-D results plotted in the toroidal midplane of the antenna with L_T = 23.5 cm and the same current (300 A in the equatorial plane) in each case. Note that the energy absorption is localized between the two-ion hybrid resonance surface (l = 4) and the fundamental ion cyclotron resonance surface, which are labeled by the dashed lines in Fig. 11. The energy deposition profile for the half-turn antenna is somewhat broader along the resonant surface than that for the compact geometry. Also, the peak power absorbed for the half-turn geometry is about 4 times that for the compact geometry with the same current. This suggests that the power deposited per unit arc length of antenna is approximately constant, since the ratio of arc lengths for the two cases is about 4. The contours of power deposition are also shown in Fig. 12, plotted in the equatorial plane, where most of the absorption occurs near the two-ion hybrid resonance surface and in the toroidal region nearest the antenna.

The complex antenna impedance Z is found from (44),(45) and is plotted in Fig. 13 for both the compact and half-turn antenna geometries. As the toroidal extent of the antenna L_T becomes less ($\pi R_T/L_T$ increases), more toroidal modes are excited and the impedance Z increases. The real part of Z corresponds to the real power absorbed by the plasma and tends to saturate more quickly at higher mode numbers than does the imaginary part of Z, which corresponds to the antenna reactance. This is because the fast-wave cutoff C = 0 moves toward the plasma center for higher toroidal mode numbers, and it becomes more difficult for the waves to

ORNL-DWG 85-3484 FED

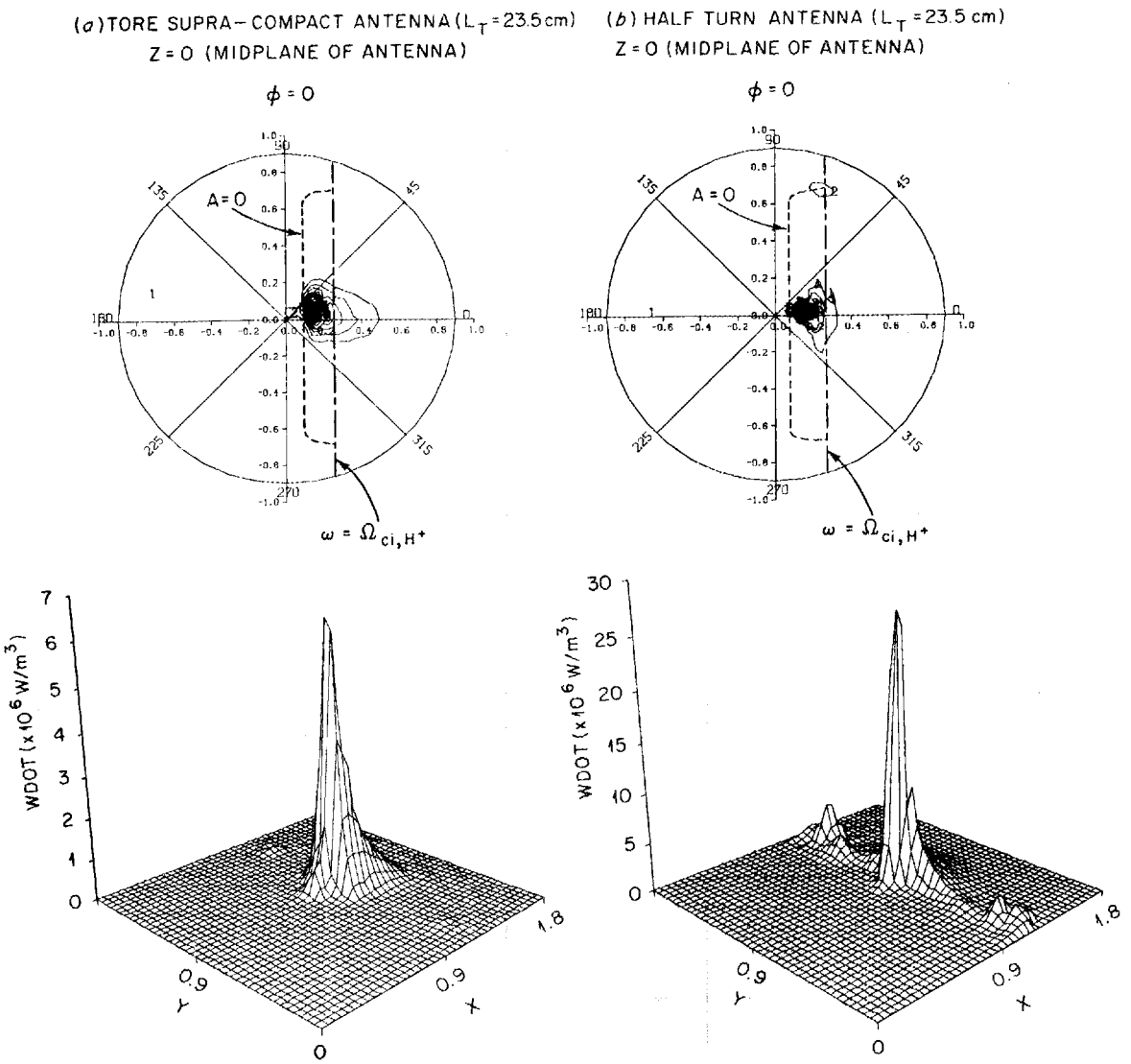

Fig. 11. Local energy absorption contours in the antenna midplane for (a) compact and (b) half-turn antennas. Antenna current in the equatorial plane is 300 A for both cases. Toroidal half-width L_T = 23.5 cm.

ORNL-DWG 85-3185 FED

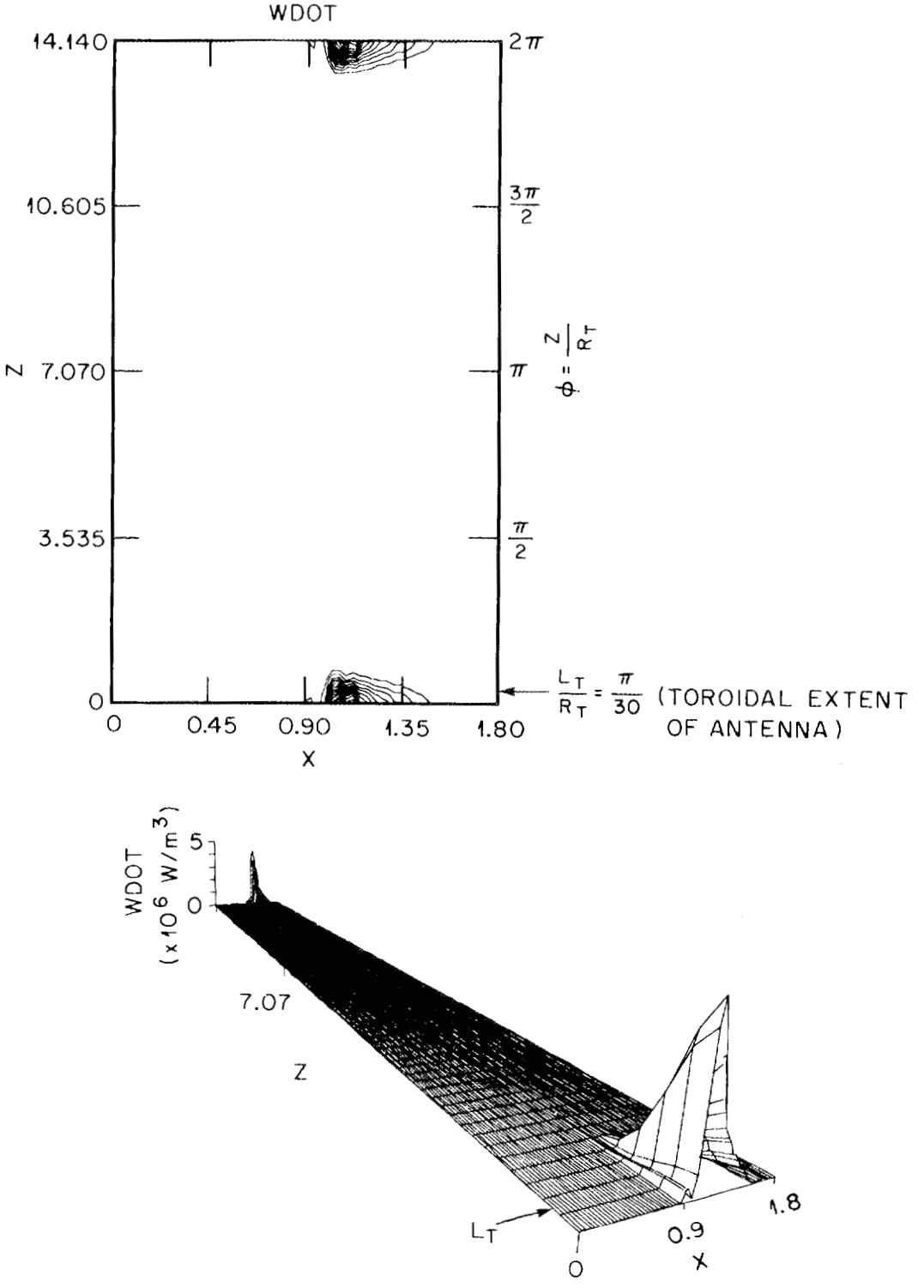

Fig. 12. r-z contours of local energy absorption for the compact antenna (case of Fig. 11).

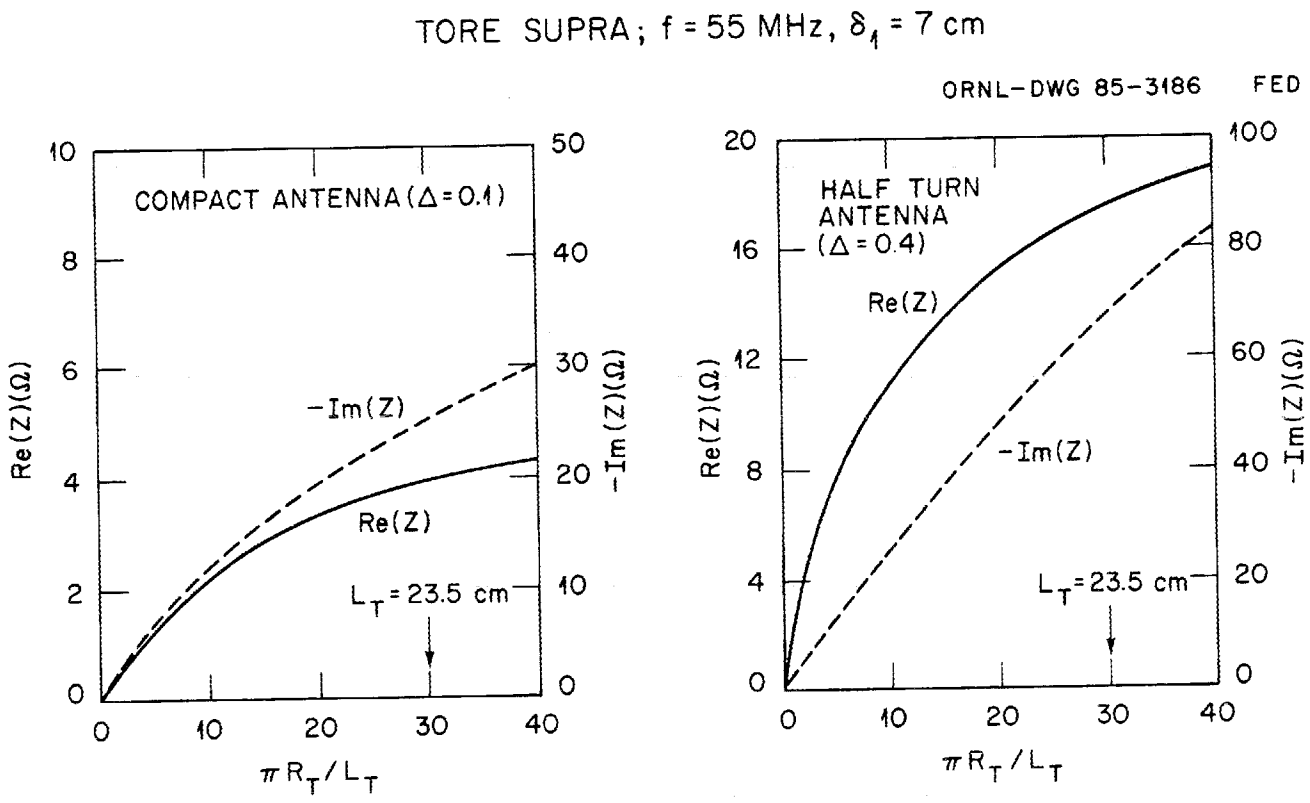

Fig. 13. Complex antenna impedance versus inverse toroidal half-length for compact and half-turn antennas.

penetrate the outer evanescent region. Thus, there is an upper limit in the toroidal mode number, above which little or no power is absorbed. The dependence on L_T is much the same for both compact and half-turn antenna geometries. The magnitude of Z, however, for the half-turn case is 3-4 times that for the compact antenna. Since the ratio of effective poloidal lengths for the two cases is about 4, we conclude that the impedance per unit length remains about constant.

Figure 14 shows the sensitivity of these results to the assumed collision frequency ν/ω. The total power absorbed $P_{abs}(k_z,\omega)$ is shown versus ν/ω for the fourth toroidal eigenmode, $l = 4$. Note that the power absorbed is practically independent of the collision frequency assumed as ν is varied over almost an order of magnitude. However, the half-width at half-maximum (HWHM) of the two-ion hybrid resonance region (HWHM/Δr) varies roughly linearly with ν, and the maximum energy deposition rate at resonance $\dot{W}_{max}$ varies inversely with ν. Thus, results that depend on total power absorbed, such as antenna impedance, are relatively insensitive to our absorption model. However, results depending on detailed knowledge of the geometry of the resonant region will depend on the exact absorption machanism.

5.2 FUNDAMENTAL ION CYCLOTRON RESONANCE IN TOKAMAKS

Next we let the fraction of the minority species (H^+) approach zero and consider a pure D_2^+ plasma with f = 27.5 MHz. Figure 15 compares the A = 0, B = 0, and C = 0 contours for this case (b) with those for the $\eta = n_{H^+}/n_{D_2^+} = 0.1$ case (a) of Figs. 4-11. Note that the fundamental ion cyclotron resonance for D_2^+ in Fig. 15(b) is near the plasma center, and the hybrid layer (A = 0) or "perpendicular ion cyclotron resonance" is at the outermost edge of the plasma. Since the density is very low at the

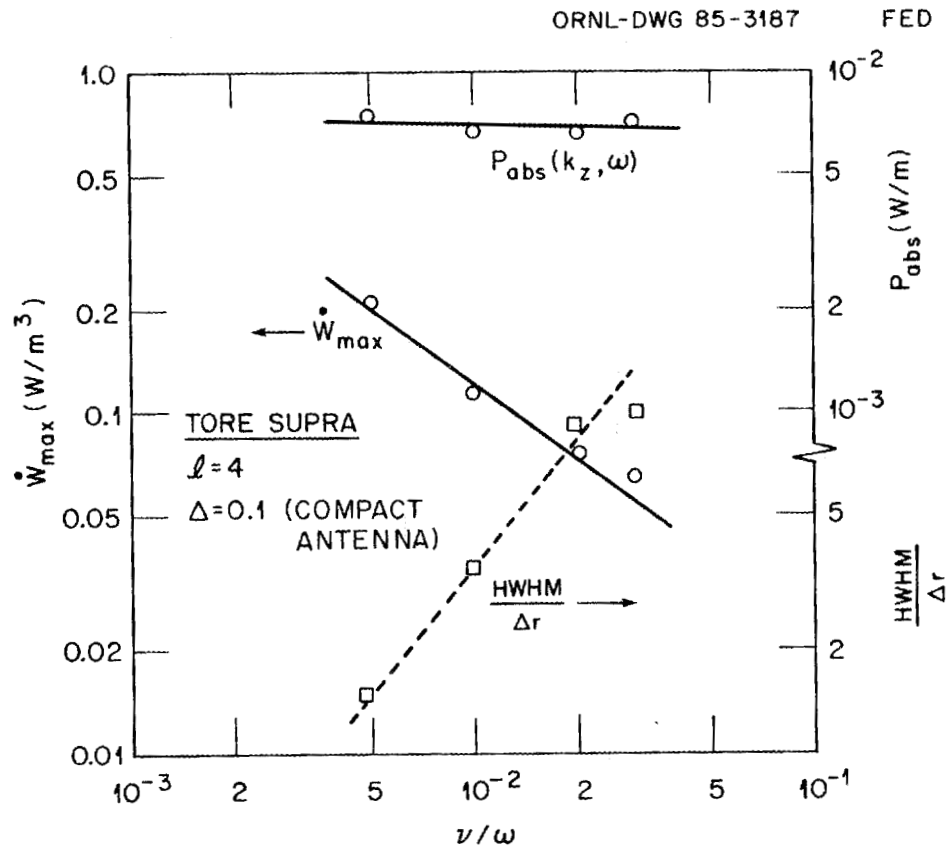

Fig. 14. Sensitivity of results to assumed collision frequency for the l = 4 toroidal mode in Tore Supra with compact antenna.

ORNL-DWG 85-3188 FED

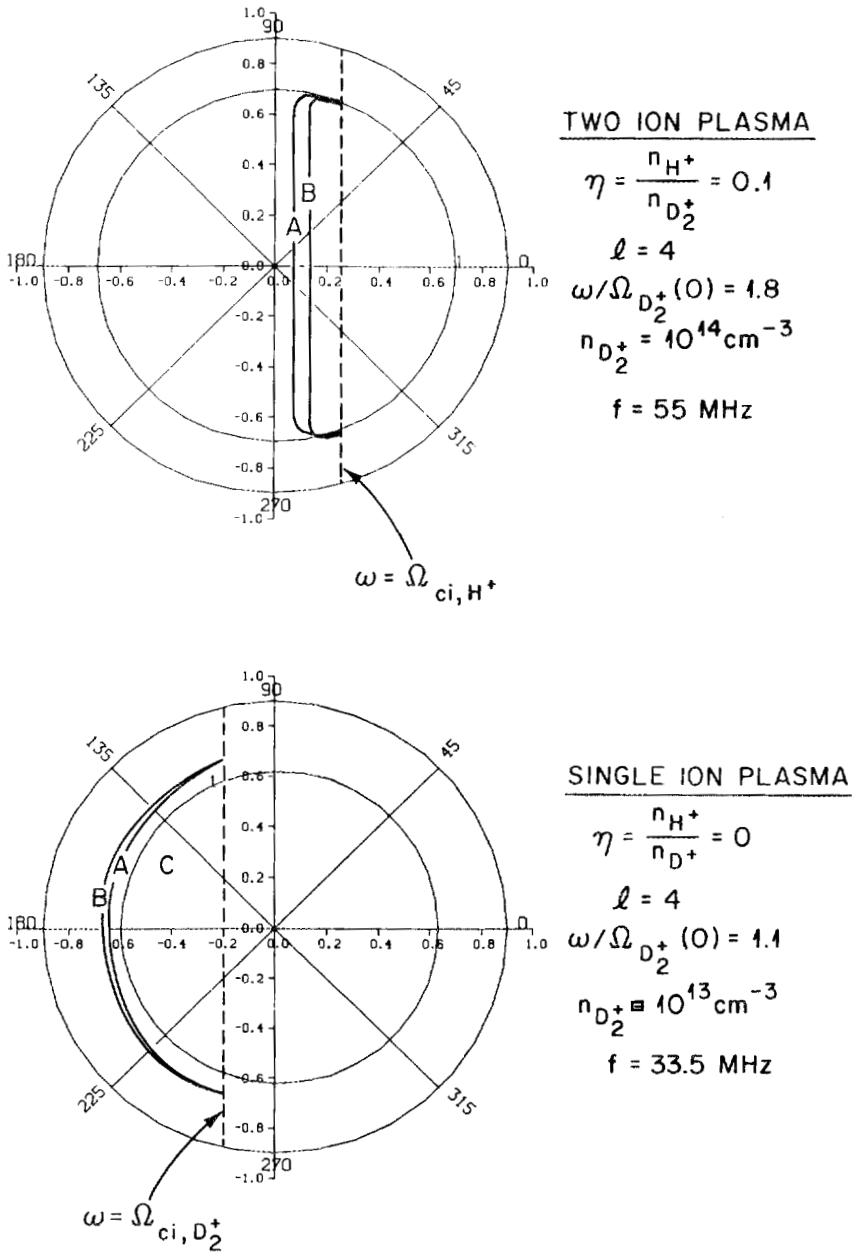

Fig. 15. Two-ion hybrid resonance layer (A), slow-wave cutoff (B), and fast-wave cutoff (C) for single- and two-ion plasmas.

plasma edge, the $A = 0$ surface leads to only a very small heating rate in this region. However, since the fundamental resonance for D_2^+ is still near the plasma center, heating at this resonance layer is of interest.

The energy deposition profiles for this case are shown in Fig. 16 for $\lambda = 1$, density $n = 10^{13}$ cm^{-3}, and the half-turn antenna on the high-field side. Note that except for two spikes in the absorption at the plasma edge, there is essentially no resonant interaction or absorption along the fundamental resonance surfaces. The reason for this is clear from (33),(34). At this density and at $\omega = \Omega_{ci}$ the terms proportional to $K_\perp$ and K_x dominate and (33), for example, gives

$$\frac{\omega^2}{c^2}K_\perp u - i\,\frac{\omega^2}{c^2}\,\frac{K_x}{b_z}\,v = 0 \ .$$

Noting that $K_x = -K_\perp$ at $\omega = \Omega_{ci}$, this is

$$E_+ = E_r + i\,\frac{E_\theta}{b_z} = 0 \ ,$$

and similarly for (34). Thus the wave at resonance is all E_- and therefore right-hand polarized. Since the ions rotate in the left-hand sense, there is no resonant interaction. For the λ^2/R_T^2 terms in (33),(34) to be comparable to the $(\omega^2/c^2)K_\perp$ term requires $n \lesssim (\lambda/R_T)^2c^2 \times (m_i\varepsilon_0/e^2)$, where e is the electron charge, or $n \lesssim 10^{11}$ cm^{-3} at $\lambda = 2$ and $n \lesssim 10^{12}$ cm^3 at $\lambda = 6$. Figure 17 shows the energy deposition for $n = 10^{11}$ cm^{-3} and $\lambda = 1$. Now a resonant interaction is clearly evident all along the fundamental resonant surface except near the equatorial plane ($y = 0$) where, from (23), $\vec{B} \cdot \nabla B$ approaches zero. Figure 18 compares

ORNL-DWG 85-3189 FED

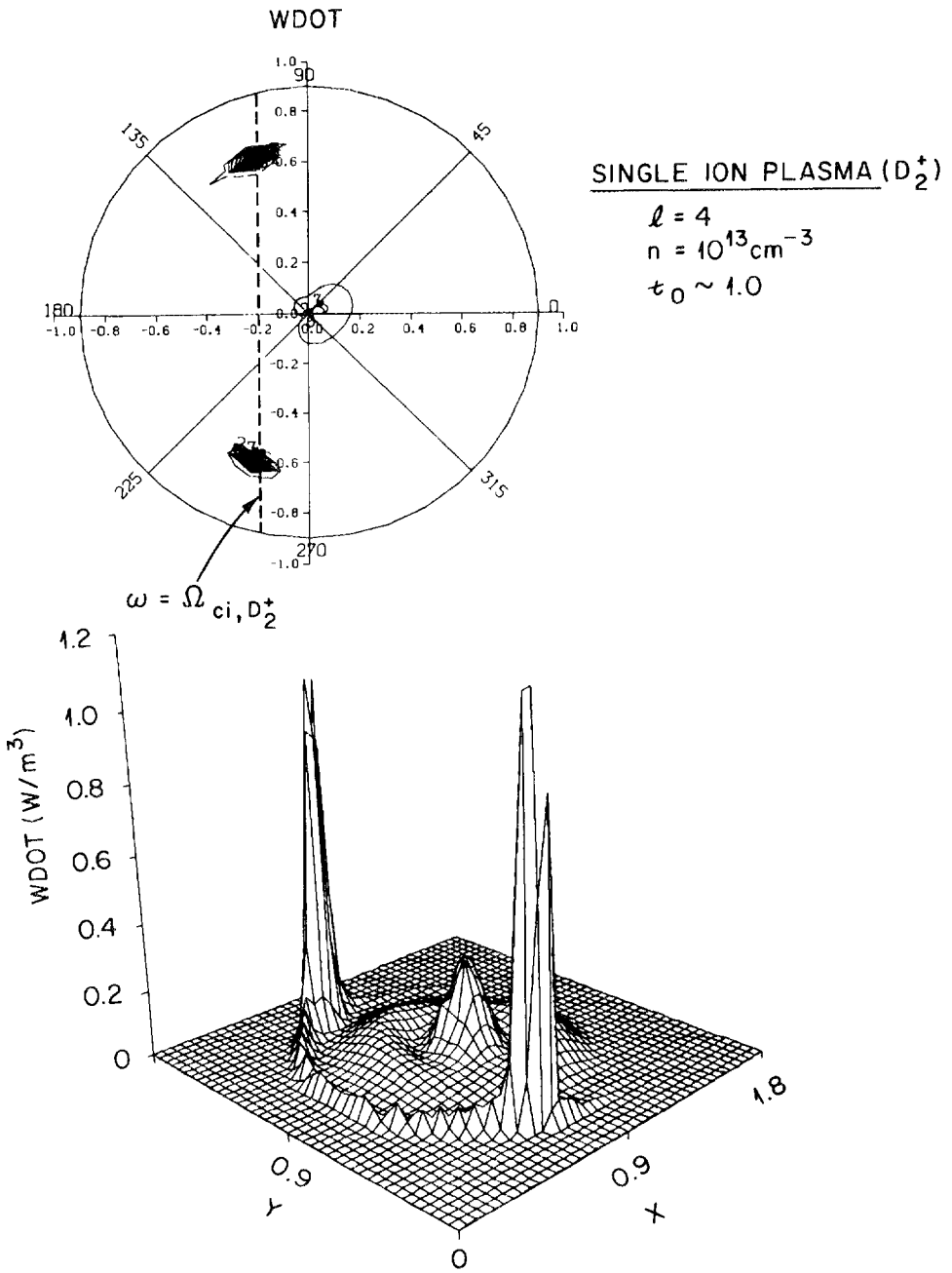

Fig. 16. Energy absorption contours for the l = 4 toroiodal mode in a single-ion plasma with $n = 10^{13}$ cm^{-3} and $\lambda_0 \cong 1.0$. The half-turn antenna is on the high-field (left) side.

ORNL-DWG 85-3190 FED

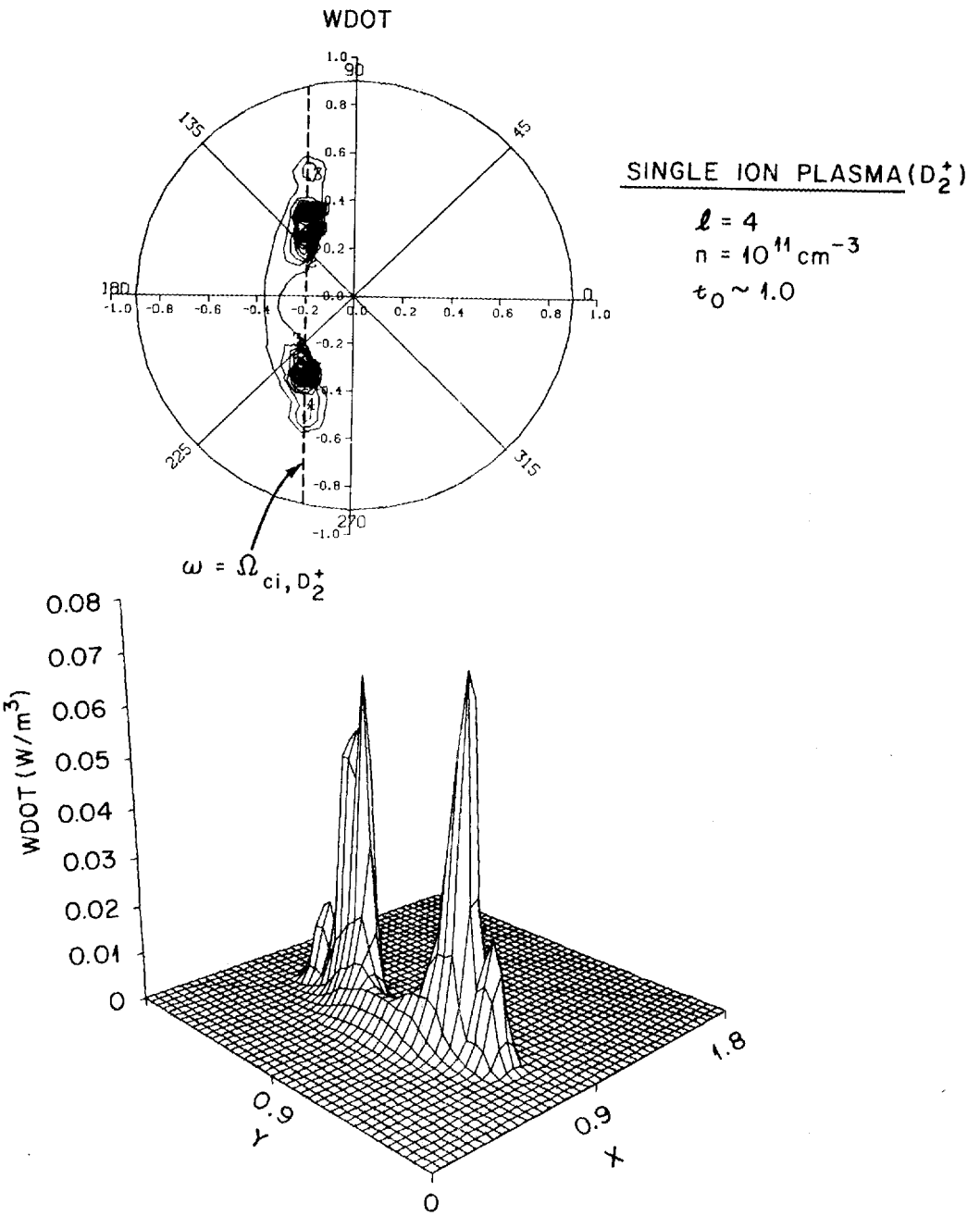

Fig. 17. The case of Fig. 16 with $n = 10^{11}\ cm^{-3}$.

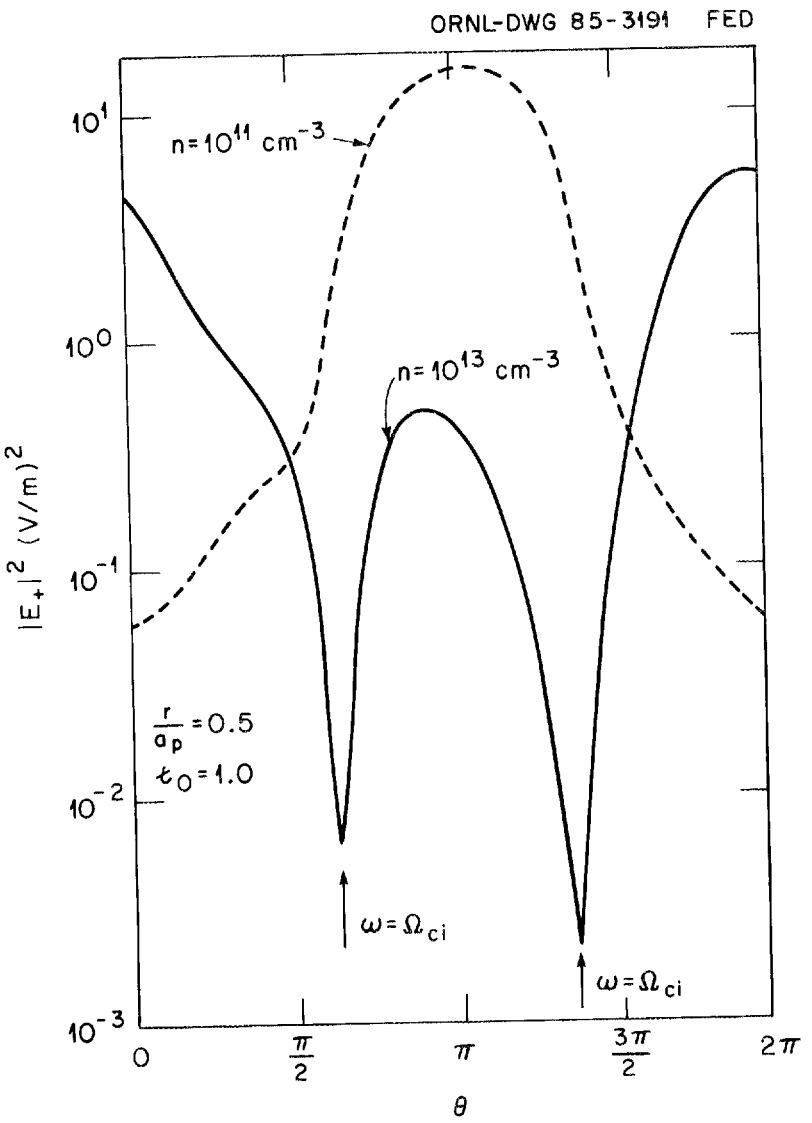

Fig. 18. $|E_+|^2$ versus poloidal angle at $r/a_p = 0.5$ for Figs. 16 and 17.

profiles of $|E_+|^2$ versus θ at $r/a_p = 0.5$ for the cases of Figs. 16 and 17. Note the strong cusps in $|E_+|^2$ at the resonance crossings in the higher-density case (solid line). For $n = 10^{11}$ cm^{-3} (dashed line) E_+ is clearly nonzero at resonance, and we therefore expect a resonant interaction, as shown in Fig. 17. Furthermore, the total power absorbed in this case is approximately proportional to λ_0 or $\vec{B} \cdot \nabla B$, as shown in Fig. 19. Thus, we conclude that for moderate to low densities and high rotational transform (so that $\vec{B} \cdot \nabla B \sim 0$ [1]), fundamental ion cyclotron resonance is possible in tokamak geometry. While this may not be of any practical importance in tokamaks, it suggests that in alternate geometries such as stellarators, where $\vec{B} \cdot \nabla B$ is naturally of order unity, direct heating at the fundamental may be possible [8,9].

6. THE POLOIDALLY SYMMETRIC MAGNETIC MIRROR

Next we consider a mirror magnetic field,

$$\vec{B}_0 = \nabla\psi \times \frac{\hat{\theta}}{r} = -\frac{1}{r}\frac{\partial\psi}{\partial z}\hat{r} + \frac{1}{r}\frac{\partial\psi}{\partial r}\hat{z} , \tag{51}$$

where $\psi(r,z)$ is the flux function

$$\psi(r,z) = \int_0^r rB_z^0 \, dr = \frac{\phi_B}{2\pi} \tag{52}$$

and $\phi_B = 2\pi\psi$ is the magnetic flux enclosed by a surface of constant pressure.

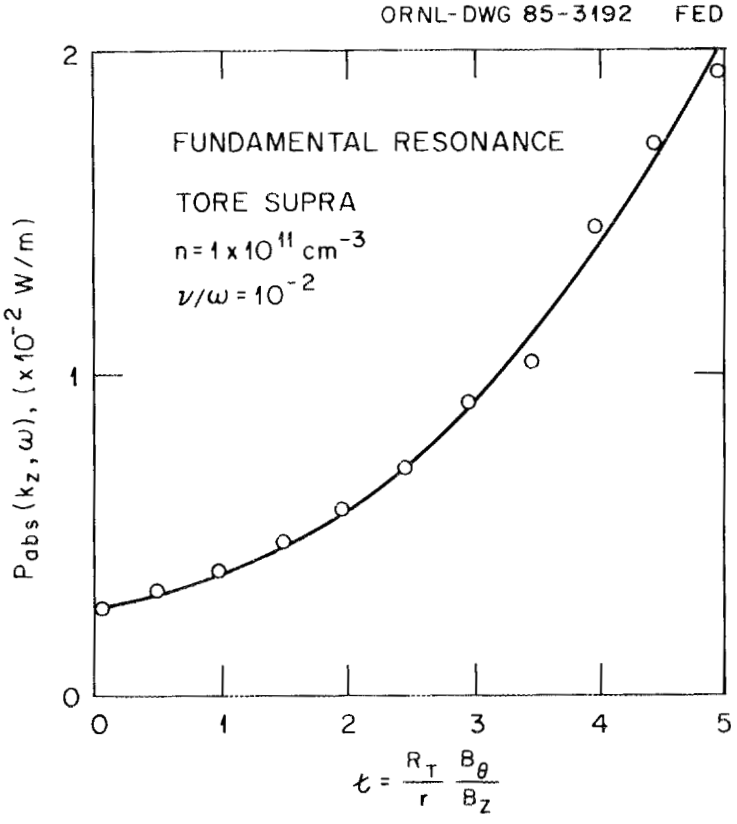

Fig. 19. Dependence of total power absorbed on rotational transform for the case of Fig. 17 ($n = 10^{11}$ cm^{-3}).

6.1 WAVE EQUATIONS FOR THE MIRROR

From (51) we have $rB_0 = |\nabla\psi|$, and the three unit vectors in (13) are

$$\hat{\delta}_1 = \nabla\hat{\psi} = b_z\hat{r} - b_r\hat{z} \ ,$$
$$\hat{\delta}_2 = \hat{b} \times \nabla\hat{\psi} = \hat{\theta} \ , \tag{53}$$
$$\hat{\delta}_3 = \hat{b} = b_r\hat{r} + b_z\hat{z} \ .$$

With (53) $\overleftrightarrow{K} \cdot \vec{E}$ in (15) becomes

$$\overleftrightarrow{K} \cdot \vec{E} = \left[K_\perp\left(b_zE_r - b_rE_z\right) - iK_xE_\theta\right]\left(b_z\hat{r} - b_r\hat{z}\right)$$
$$+ \left[K_\perp E_\theta + iK_x\left(b_zE_r - b_rE_z\right)\right]\hat{\theta} + K_\parallel\left[b_rE_r + b_zE_Z\right]\left(b_r\hat{r} + b_z\hat{z}\right) \ . \tag{54}$$

Assuming $\hat{b} \cdot \vec{E} = 0$, we have

$$E_z = -\frac{b_r}{b_z}E_r \ , \tag{55}$$

and (54) simplifies to

$$\overleftrightarrow{K} \cdot \vec{E} = \left(K_\perp E_r - iK_xb_zE_\theta\right)\left(\hat{r} - \frac{b_r}{b_z}\hat{z}\right) + \left(K_\perp E_\theta + \frac{iK_x}{b_z}E_r\right)\hat{\theta} \ . \tag{56}$$

Now we write (7) in r,θ,z and use (55) to eliminate E_z,

$$-\frac{1}{r}\frac{\partial}{\partial\theta}\left(\frac{1}{r}\frac{\partial}{\partial r}rE_\theta - \frac{1}{r}\frac{\partial E_r}{\partial\theta}\right) + \frac{\partial}{\partial z}\left[\frac{\partial E_r}{\partial z} + \frac{\partial}{\partial r}\left(\frac{b_rE_r}{b_z}\right)\right] + \frac{\omega^2}{c^2}\left(\overleftrightarrow{K} \cdot \vec{E}\right)_r$$
$$= -i\omega\mu_0J_r \ ,$$

$$\frac{\partial}{\partial z}\left[\frac{1}{r}\frac{\partial}{\partial\theta}\left(\frac{b_r}{b_z}E_r\right)+\frac{\partial E_\theta}{\partial z}\right]+\frac{\partial}{\partial r}\left(\frac{1}{r}\frac{\partial}{\partial r}rE_\theta-\frac{1}{r}\frac{\partial E_r}{\partial\theta}\right)+\frac{\omega^2}{c^2}\left(\overleftrightarrow{K}\cdot\vec{E}\right)_\theta \tag{57}$$

$$= -i\omega\mu_0 J_\theta ,$$

$$-\frac{1}{r}\frac{\partial}{\partial r}r\left[\frac{\partial E_r}{\partial z}+\frac{\partial}{\partial r}\left(\frac{b_r E_r}{b_z}\right)\right]-\frac{1}{r}\frac{\partial}{\partial\theta}\left[\frac{1}{r}\frac{\partial}{\partial\theta}\left(\frac{b_r}{b_z}E_r\right)+\frac{\partial E_\theta}{\partial z}\right]+\frac{\omega^2}{c^2}\left(\overleftrightarrow{K}\cdot\vec{E}\right)_z$$

$$= -i\omega\mu_0 J_z .$$

Fourier analyzing in the θ direction with

$$E(r,\theta,z) = \sum_m E_m(r,z)e^{im\theta} , \tag{58}$$
$$J(r,\theta,z) = \sum_m J_m(r,z)e^{im\theta} ,$$

and combining the $\hat{r}$ and $\hat{z}$ equations to give the $\hat{\delta}_1 = \nabla\hat{\psi}$ component:

$$-\frac{im}{r}\left(\frac{1}{r}\frac{\partial}{\partial r}rE_\theta-\frac{imE_r}{r}\right)+\frac{\partial}{\partial z}\left[\frac{\partial E_r}{\partial z}+\frac{\partial}{\partial r}\left(\frac{b_r E_r}{b_Z}\right)\right]$$

$$+\frac{\omega^2}{c^2}\left[\left(\overleftrightarrow{K}\cdot\vec{E}\right)_r-\frac{b_r}{b_z}\left(\overleftrightarrow{K}\cdot\vec{E}\right)_z\right]$$

$$-\frac{b_r}{b_z}\left\{-\frac{1}{r}\frac{\partial}{\partial r}r\left[\frac{\partial E_r}{\partial z}+\frac{\partial}{\partial r}\left(\frac{b_r E_r}{b_z}\right)\right]-\frac{im}{r}\left[\frac{im}{r}\left(\frac{b_r}{b_z}E_r\right)+\frac{\partial E_\theta}{\partial z}\right]\right\}$$

$$= -i\omega\mu_0\left(J_{r,m}-\frac{b_r}{b_z}J_{Z,m}\right) ,$$

$$\frac{\partial}{\partial z}\left[\frac{im}{r}\frac{b_r}{b_z}E_r+\frac{\partial E_\theta}{\partial z}\right]+\frac{\partial}{\partial r}\left[\frac{1}{r}\frac{\partial}{\partial r}rE_\theta-\frac{imE_r}{r}\right]+\frac{\omega^2}{c^2}\left(\overleftrightarrow{K}\cdot\vec{E}\right)_\theta$$

$$= -i\omega\mu_0 J_{\theta,m} , \tag{59}$$

where we have dropped the subscript m from $\vec{E}$ for brevity. Defining $u = rE_r$ and $v = rE_\theta$ and using (56), the final set of two differential equations for the axisymmetric mirror is

$$\frac{\partial^2 u}{\partial z^2} + \frac{r}{R}\frac{\partial^2 \alpha u}{\partial r \partial z} + \left(\frac{\omega^2}{c^2}K_\perp - \frac{m^2}{r^2}\right)\frac{1}{b_z^2}u - i\frac{\omega^2}{c^2}\frac{K_x}{b_z}v - \frac{im}{r}\frac{\partial v}{\partial r}$$

$$+ \frac{\alpha}{R}\left(r\frac{\partial^2 u}{\partial r \partial z} + \frac{r}{R}\frac{\partial}{\partial r}r\frac{\partial \alpha u}{\partial r} + im\frac{\partial v}{\partial z}\right) = -i\omega\mu_0 r\left(J_{r,m} - \frac{\alpha r}{R}J_{z,m}\right) , \tag{60}$$

$$r\frac{\partial}{\partial r}\left(\frac{1}{r}\frac{\partial v}{\partial r}\right) + \frac{\partial^2 v}{\partial z^2} + \left(\frac{\omega^2}{c^2}K_\perp\right)v + i\frac{\omega^2}{c^2}\frac{K_x}{b_z}u - im\left[r\frac{\partial}{\partial r}\left(\frac{u}{r^2}\right) - \frac{1}{R}\frac{\partial \alpha u}{\partial z}\right]$$

$$= -i\omega\mu_0 r J_{\theta,m} , \tag{61}$$

where we have defined

$$\alpha \equiv \frac{b_r R}{b_z r} , \tag{62}$$

and R is the radius of the metal wall. We take the tangential component of $\vec{E}$ to vanish at $r = R$ and $z = 0,L$, where L is the distance between mirrors. This gives $u = v = 0$ at $z = 0,L$ and $v = 0$ at $r = R$. From (55), $u = 0$ at $r = R$ also, since $E_z = 0$ there. By definition, u and v vanish at $r = 0$.

6.2 MODEL MIRROR MAGNETIC FIELD

To solve (60),(61) we choose the mirror flux function in (52) to be

$$\psi(r,z) = B_0\left[\frac{1}{2}r^2 - \frac{\varepsilon}{k}rI_1(kr)\cos k\left(z - \frac{L}{2}\right)\right] , \tag{63}$$

where I_1 is the modified Bessel function of the first kind of order one, $k = 2\pi/L$, and L is the distance between mirrors. With (51) and $[xI_1(x)]' = xI_0(x)$, we have

$$B_r^0(r,z) = -\frac{1}{r}\frac{\partial\psi}{\partial z} = -B_0\varepsilon I_1(kr)\sin k\left(z - \frac{L}{2}\right) ,$$

$$B_Z^0(r,z) = \frac{1}{r}\frac{\partial\psi}{\partial r} = B_0\left[1 - \varepsilon I_0(kr)\cos k\left(z - \frac{L}{2}\right)\right] . \tag{64}$$

Thus the coefficient ε is related to the mirror ratio M by

$$M = \frac{B_Z^0(0,0)}{B_Z^0\left(0,\frac{L}{2}\right)} = \frac{1 + \varepsilon}{1 - \varepsilon} .$$

The coefficient α that occurs in (60), (61) is

$$\alpha \equiv \frac{B_r}{B_z}\frac{R}{r} = \begin{cases} -\dfrac{R}{r}\left[\dfrac{\varepsilon I_1(kr)\sin k\left(z - \frac{L}{2}\right)}{1 - \varepsilon I_0(kr)\cos k\left(z - \frac{L}{2}\right)}\right] , & r > 0 \\[2ex] -\dfrac{kR}{2}\left[\dfrac{\varepsilon \sin k\left(z - \frac{L}{2}\right)}{1 - \varepsilon \cos k\left(z - \frac{L}{2}\right)}\right] , & r = 0 \end{cases} . \tag{65}$$

Figure 20 shows (a) contours of constant ψ (field lines) and (b) mod-B from (63),(64) for $M = 1.4$ and $\varepsilon = 1/6$.

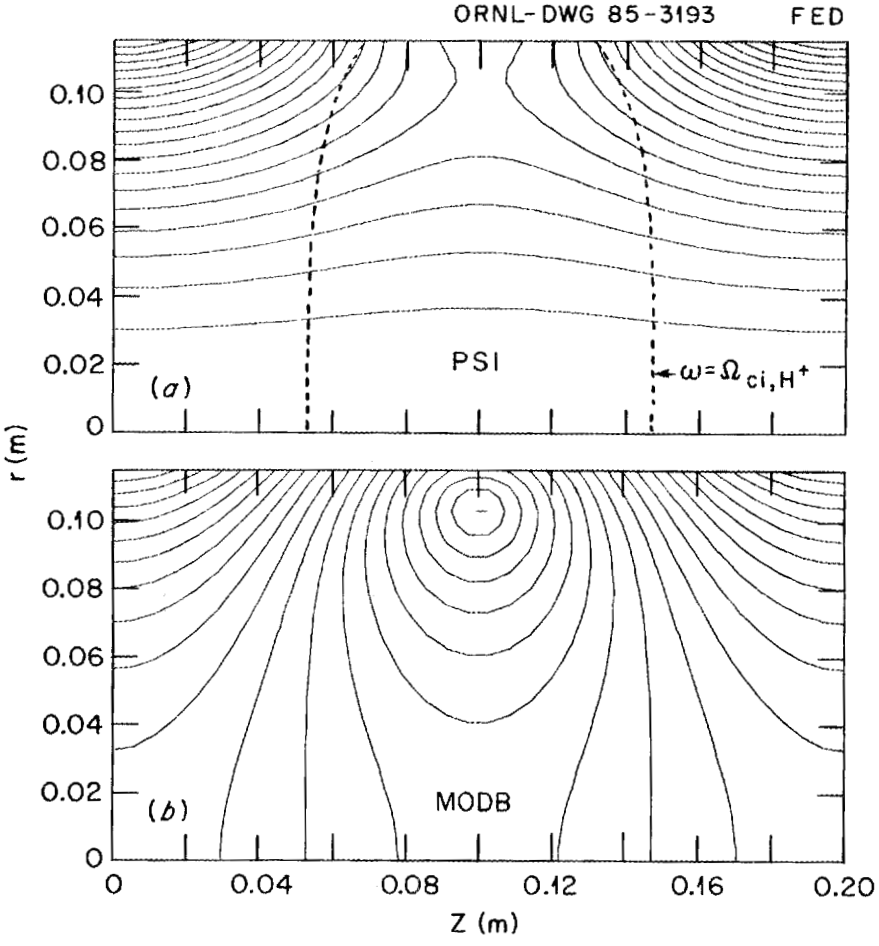

Fig. 20. (a) Magnetic field lines and (b) contours of |B| for mirror ratio M = 1.4.

From (64) we find $\nabla \cdot \vec{B} = 0$, $\nabla \times \vec{B} = 0$, and

$$\vec{B} \cdot \nabla B = b_Z^2 |B| \left[\frac{\partial B_z^0}{\partial z} + 2\frac{\alpha r}{R} \frac{\partial B_z^0}{\partial r} + \left(\frac{\alpha r}{R}\right)^2 \frac{\partial B_r^0}{\partial r} \right]$$

where

$$\frac{\partial B_z^0}{\partial z} = B_0 \varepsilon k I_0(kr) \sin k\left(z - \frac{L}{2}\right) ,$$

$$\frac{\partial B_z^0}{\partial r} = -kB_0 \varepsilon I_1(kr) \cos k\left(z - \frac{L}{2}\right) ,$$

$$\frac{\partial B_r^0}{\partial r} = -B_0 \varepsilon \left[kI_0(kr) - \frac{I_1(kr)}{r} \right] \sin k\left(z - \frac{L}{2}\right) .$$

6.3 ANTENNA CURRENT FOR THE POLOIDALLY SYMMETRIC MIRROR

We assume a current distribution

$$\vec{J}(r,\Theta,z) = \frac{I_0 \delta(r - r_0)}{L_z} f_z(z) f_{(\Theta)} \hat{\Theta} , \tag{66}$$

where $f(\Theta)$ is given by (50) with $p = 0$ and $f_z(z)$ is taken to be a Gaussian centered at $z = z_0$ with width L_z:

$$f_z(z) = \frac{\exp\left[- \frac{(z - z_0)^2}{L_z{}^2} \right]}{\frac{\sqrt{\pi}}{2} \left[\operatorname{erf}\left(\frac{z_0}{L_z}\right) + \operatorname{erf}\left(\frac{L/2 - z_0}{L_z}\right) \right]} . \tag{67}$$

Equation (67) is normalized so that $\int_0^{L/2} f(z)dz = L_z$. Thus, from (66), $\int dr \int dz\, \vec{J}(r,\theta,z) = I_0 f(\theta)\hat{\theta}$. We Fourier expand (50) with p = 0 to give

$$f(\theta) = f_0 \sum_{n=-\infty}^{\infty} \exp\left[-\left(\frac{\theta - 2\pi n}{\pi\Delta}\right)^2\right] \sim \frac{f_0\sqrt{\pi\Delta}}{2} \sum_{m=-\infty}^{\infty} \exp\left[-\frac{m^2(\pi\Delta)^2}{4} + im\theta\right], \tag{68}$$

where f_0 is chosen to make the maximum value of $f(\theta)$ unity. Thus (58) gives

$$\vec{J}_m(r,z) = \frac{I_0\delta(r - r_0)}{L_z} f_z(z) \frac{f_0\sqrt{\pi\Delta}}{2} \exp\left[\frac{-m^2(\pi\Delta)^2}{4}\right] \hat{\theta} . \tag{69}$$

In practice we solve (60) and (61) with $I_0 = 1$ and $m = 0$ so from (68), $f_0\sqrt{\pi\Delta}/2 = 1$ and

$$\vec{J}_m(r,z) = \frac{\delta(r - r_0)}{L_z} f_z(z)\, \hat{\theta} . \tag{70}$$

6.4 LOCAL ENERGY DEPOSITION AND ANTENNA IMPEDANCE IN THE MIRROR

From (17) with $\nabla\hat{\psi} = b_z\hat{r} - b_r\hat{z}$, $\hat{b} \times \nabla\hat{\psi} = \hat{\theta}$, and $\hat{b} = b_r\hat{r} + b_z\hat{z}$, we have

$$\vec{J}_{plasma} = \overleftrightarrow{\sigma} \cdot \vec{E} = \left[\sigma_\perp(b_z E_r - b_r E_\theta)\right) + \sigma_x E_\theta\right]\left(b_z\hat{r} - b_r\hat{z}\right)$$

$$+\left[\sigma_\perp E_\theta - \sigma_x\left(b_z E_r - b_r E_z\right)\right]\hat{\theta} + \sigma_\parallel\left(b_r E_r + b_z E_z\right)\left(b_r\hat{r} + b_z\hat{z}\right)$$

and

$$\vec{E}^* \cdot \vec{J}_{plasma} = \vec{E}^* \cdot \overleftrightarrow{\sigma} \cdot \vec{E} = \sigma_\perp |E_\perp|^2 + \sigma_\parallel |E_\parallel|^2 + \sigma_x 2i \text{ Im } E_\psi^* E_\theta \ , \tag{71}$$

where

$$E_\parallel = \hat{b} \cdot \vec{E} = b_r E_r + b_z E_z = 0 \ ,$$

$$E_\psi = \nabla\hat{\psi} \cdot \vec{E} = b_z E_r - b_r E_z = \frac{E_r}{b_z} \ ,$$

$$|E_\perp|^2 = E_\psi^* E_\psi + E_\theta^* E_\theta \ .$$

Substituting (71) into (35) and using (16) gives

$$\dot{W}(r,z) = \frac{1}{2}\omega\varepsilon_0 \left[\text{Im}(K_\perp - 1)|E_\perp|^2 + 2 \text{ Im}(K_x) \text{Im } E_\psi^* E_\theta + \text{Im } K_\parallel |E_\parallel|^2 \right] \ . \tag{72}$$

Now define E_+ and E_- to be the left- and right-hand polarized waves, respectively, for the mirror:

$$E_+ = E_\psi + iE_\theta \text{ (LHP)} \ ,$$

$$E_- = E_\psi - iE_\theta \text{ (RHP)} \ .$$

Then using (40), (72) can be written equivalently as in (41).

Integrating $\dot{W}(r,z)$ over r and z gives the power absorbed for one poloidal mode, i.e., one m:

$$P_{abs,m}(m,\omega) = \int r \, dr \int dz \, \dot{W}(r,z) \ .$$

The total power absorbed is found by summing over all m and integrating around the poloidal circumference 2π. Dividing by $|I|^2/2$ gives the loading resistance $\hat{R}(\omega)$,

$$\hat{R}(\omega) = \frac{2P_{tot}}{|I|^2} = \frac{2}{|I|^2}\, 2\pi \sum_m P_{abs}(m,\omega) \ .$$

7. NUMERICAL RESULTS FOR THE MAGNETIC MIRROR

In this section, we display numerical results for the mirror magnetic field of (63),(64). Figure 21 shows schematically the geometry treated. The plasma with density constant along field lines is contained within a perfectly conducting metal cylinder with metal end plates. Again, there may be a vacuum or a low-density plasma between the mirror plasma and the wall. A poloidal current $\vec{J}_{RF}$ models the antenna and can have arbitrary axial (z) and poloidal (Θ) extent. L_z is the axial half-width. Figure 21(b) shows the assumed axial profile for the antenna current. Equations (60), (61) are solved in this geometry by finite differencing on a mesh of 36 axial and 30 radial points. For Figs. 22 and 23 we take parameters corresponding to the local mirror in one-half the field period of the L-2 stellarator [8, 9, 13], i.e.,

$L = 0.20$ m ,

$a_{wall} = 17.5$ cm ,

$B_0 = 1.2$ T ,

$M = 1.4 \quad (\varepsilon = 1/6)$,

$n_{D_2^+} = 5 \times 10^{12}$ cm^{-3} ,

$n_{H^+} = 5 \times 10^{12}$ cm^{-3} ,

$f \sim 18$ MHz .

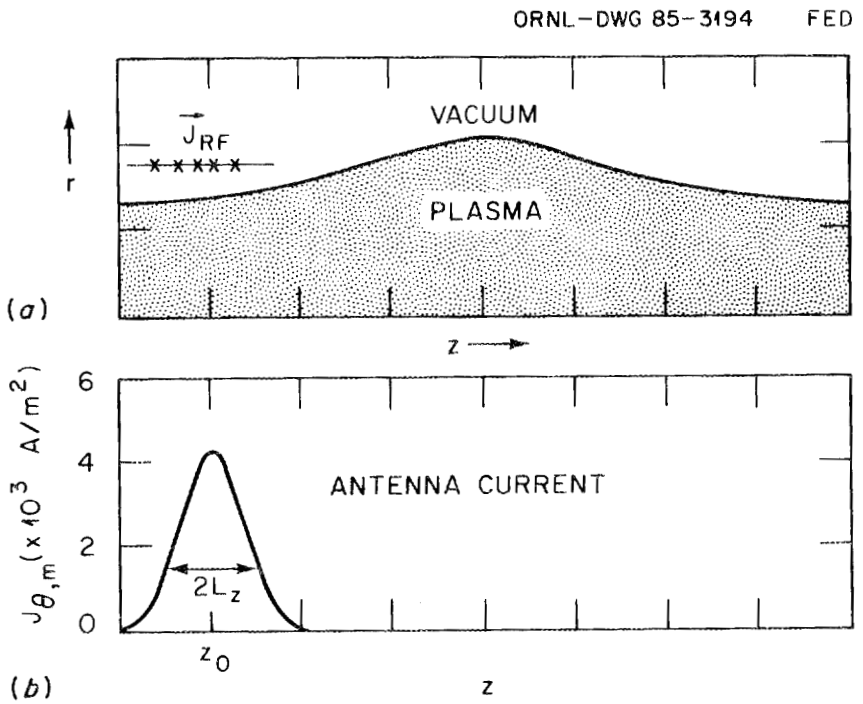

Fig. 21. (a) Mirror geometry and (b) assumed axial profile for antenna current.

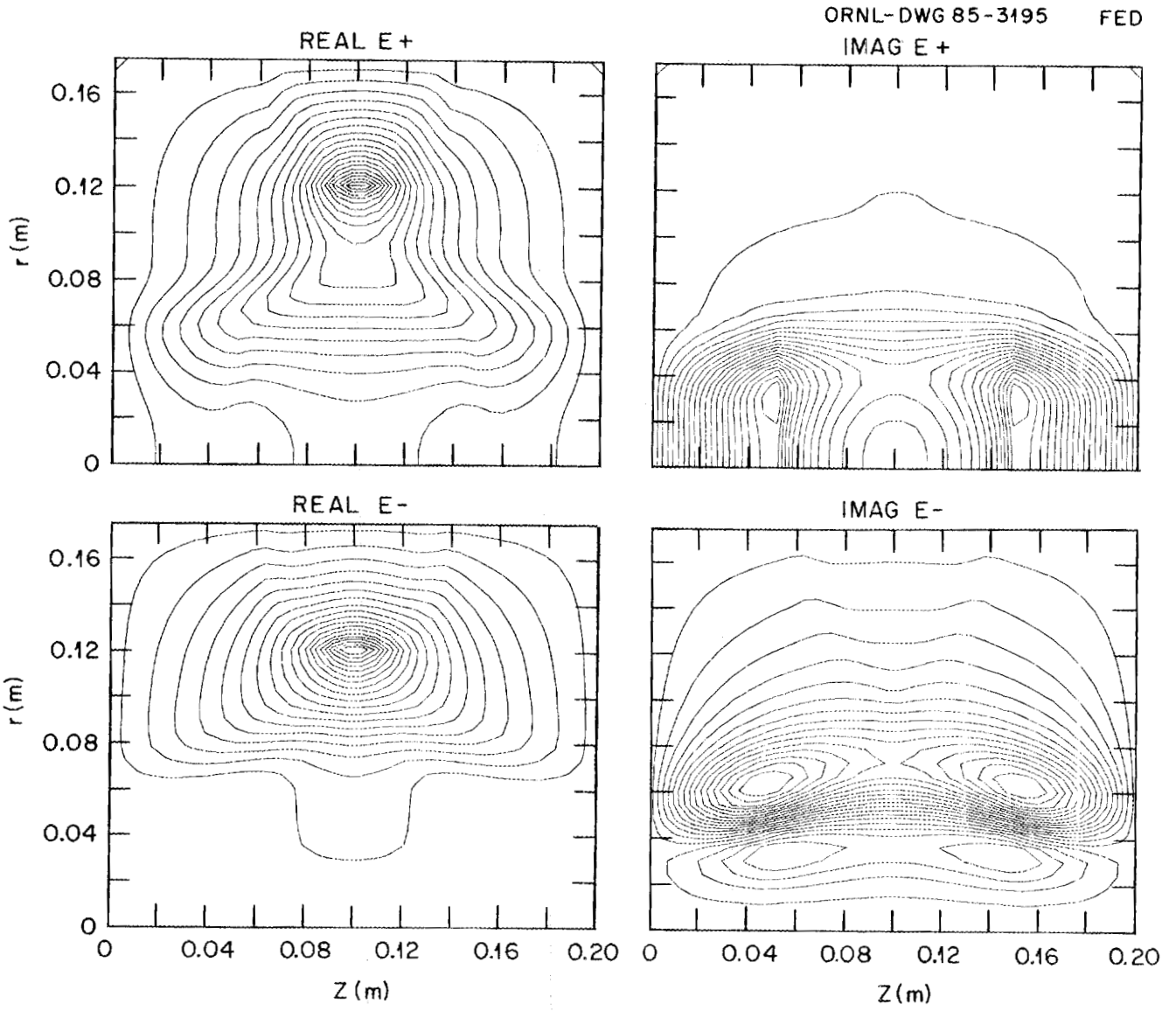

Fig. 22. Electric field contours for the m = -1 poloidal mode in a mirror with parameters corresponding to one-half the field period of the L-2 stellarator [8, 9, 13].

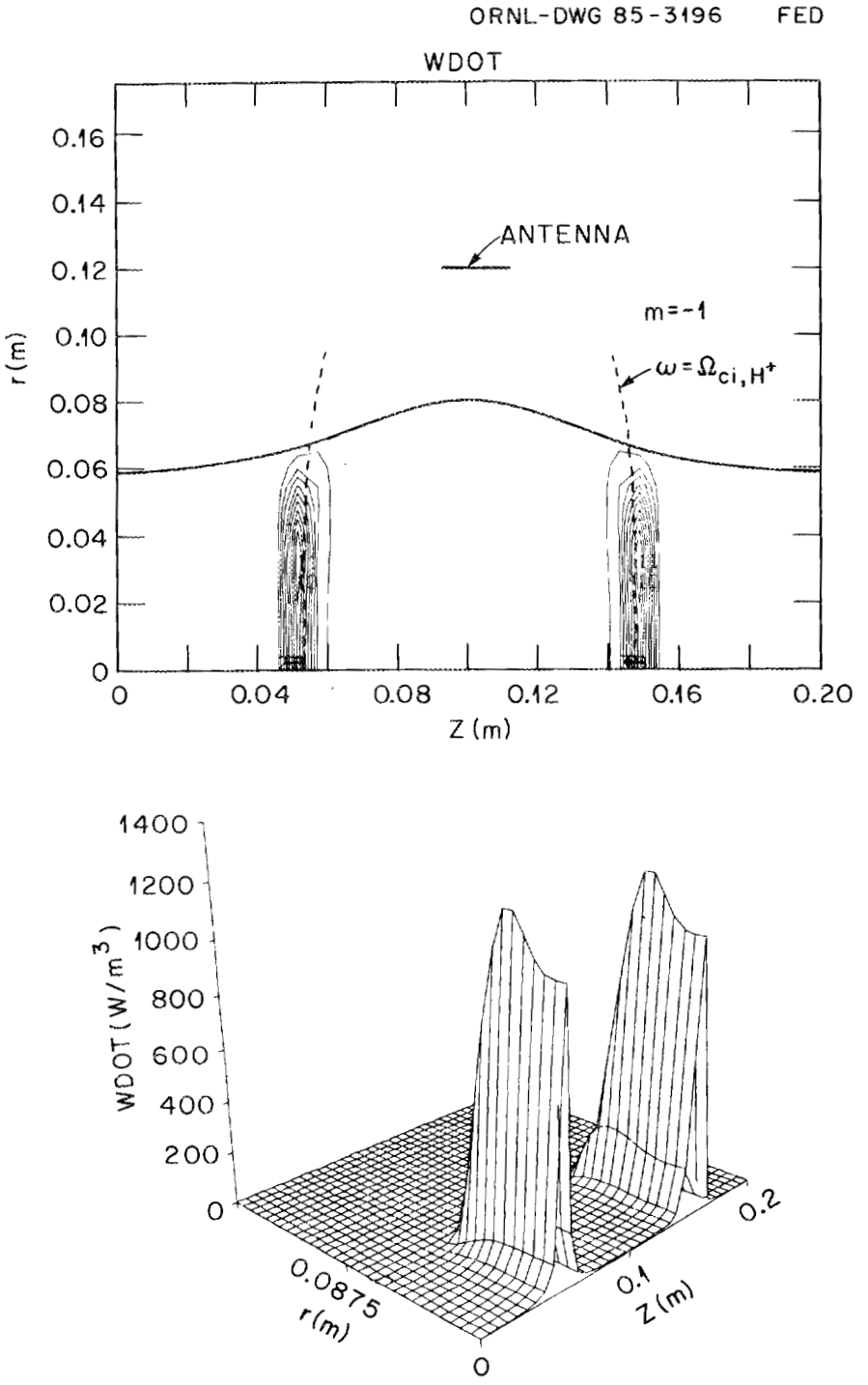

Fig. 23. Local energy absorption contours for the case of Fig. 22.

The plasma radius in the midplane is assumed to be $\rho \sim 10$ cm. For this choice of frequency, the fundamental ion cyclotron resonance surfaces for H^+ are at the locations shown in Fig. 20(a). Figure 22 shows contours of E_+ and E_- for the $m = -1$ poloidal mode with the antenna in the mirror midplane and located about 2 cm from the plasma surface. Again, E_- tends to penetrate the plasma more easily than does E_+. The deposition profiles in Fig. 23 show absorption at both fundamental resonance layers for H^+. The value of $\vec{B} \cdot \nabla B/B_0^2$ at resonance and $r/a_{wall} \sim 0.31$ is ~13.2. Although Fig. 23 shows a great deal of energy deposited at the fundamental, this result cannot be taken too seriously for the L-2 stellarator, because the boundary condition that $E_{tangential} = 0$ at $z = 0,L$ is not realistic for the stellarator. A more correct result must await solution of the wave equation for the helically symmetric stellarator.

8. DISCUSSION

The calculations reported here extend the full-wave treatment of ICRF wave propagation in tokamak and mirror geometries to include more realistic magnetic field models than have previously been used [1, 2, 3, 6]. For the tokamak we find that including the effects of large poloidal magnetic fields leads to asymmetry in the toroidal direction as well as energy absorption at the fundamental ion cyclotron resonance. This absorption is approximately proportional to the gradient in $|B|$ along $\vec{B}$ and thus to the rotational transform. However, for high plasma densities, the left-hand polarized component E_+ is shielded out of the plasma, while E_- penetrates. In this case, absorption at the fundamental occurs only near the plasma surface. For densities low enough or rotational transforms great enough that $\lambda > (R_T/c)\omega_{pi}$, the absorption

extends into the plasma and heating occurs all along the fundamental resonant surface. For minority heating of tokamaks at the two-ion hybrid frequency, we find that compact antenna designs may be as effective in heating as half-turn loops; that is, power deposited per unit length of antenna in the poloidal direction is approximately constant. Furthermore, when there is a low-density background plasma between the wall and the main plasma, undesirable vacuum cavity modes are completely suppressed and large electric fields near the wall do not occur except near the antenna. For the mirror magnetic field, both radial and axial variations in $|B|$ lead to gradients in $|B|$ along $\vec{B}$ and thus to resonant absorption at the fundamental. For parameters corresponding to the local mirror in one-half the field period of the L-2 stellarator, the $m = -1$ poloidal mode exhibits large values of $|E_+|$ near plasma center and thus strong absorption at the fundamental resonance there.

Both the mirror and tokamak calculations described in this paper may be considered preliminary evidence of possible direct fundamental resonant absorption in stellarators. In fact, the stellarator magnetic field contains elements of both the mirror and tokamak geometries. But boundary conditions and the exact magnitude of the local mirror ratio and rotational transform are sufficiently different in the stellarator case that a complete solution for the stellarator geometry is still required. For the helically symmetric stellarator field, the helical symmetry allows Fourier expansion in one ignorable coordinate, and a direct extension of the work in this paper is possible. Such a calculation is currently in progress.

REFERENCES

[1] K. Itoh, S. Itoh, and A. Fukuyama, Nucl. Fusion 24 (1984) 13.

[2] P. L. Colestock and R. F. Kluge, Bull. Am. Phys. Soc. 27 (1982) 1076; R. J. Kashuba, D. N. Smithe, and P. L. Colestock, Bull. Am. Phys. Soc. 29 (1984) 1398.

[3] P. L. Colestock and R. J. Kashuba, Nucl. Fusion 23 (1983) 763.

[4] R. S. Elet, D. Q. Hwang, and C. K. Phillips, Bull. Am. Phys. Soc. 29 (1984) 1336.

[5] K. Appert, T. Hellsten, J. Vaclavik, and L. Villard, Bull. Am. Phys. Soc. 29 (1984) 1399.

[6] B. McVey, ICRF Antenna Coupling Theory for a Cylindrically Stratified Plasma, Massachusetts Institute of Technology Plasma Fusion Center Report PFC/RR-84-12 (1984).

[7] M. W. Phillips and A. M. M. Todd, Bull. Am. Phys. Soc. 29 (1984) 1189.

[8] L. M. Kovrizhnykh and P. E. Moroz, Sov. Phys. JETP 60 (1984) 946.

[9] V. A. Batyuk, M. A. Blakh, and S. E. Grebenshchikov, in: Proceedings of the 11th European Conference on Controlled Fusion and Plasma Physics, Aachen, 1983 (Pergamon, New York, 1983) p. 373.

[10] T. H. Stix, The Theory of Plasma Waves (McGraw-Hill, New York, 1962).

[11] F. W. Perkins, "ICRF Heating Theory," IEEE Trans. Plasma Sci. PS-19 (1984) 53.

[12] J. Adam, private communication.

[13] L. M. Kovrizhnykh and P. E. Moroz, Sov. Phys. Tech. Phys. 29 (1984) 384.

ORNL/TM-9788
Dist. Category UC-20g

INTERNAL DISTRIBUTION

1. D. B. Batchelor
2. R. A. Dory
3–7. E. F. Jaeger
8. J. H. Whealton
9. H. H. Haselton
10. J. Sheffield
11–12. Laboratory Records Department
13. Laboratory Records, ORNL-RC
14. Document Reference Section
15. Central Research Library
16. Fusion Energy Division Library
17–18. Fusion Energy Division Publications Office
19. ORNL Patent Office

EXTERNAL DISTRIBUTION

20. Office of the Assistant Manager for Energy Research and Development, U.S. Department of Energy, Oak Ridge Operations Office, P.O. Box E, Oak Ridge, TN 37831
21. J. D. Callen, Department of Nuclear Engineering, University of Wisconsin, Madison, WI 53706
22. R. W. Conn, Department of Chemical, Nuclear, and Thermal Engineering, University of California, Los Angeles, CA 90024
23. S. O. Dean, Director, Fusion Energy Development, Science Applications, Inc., 2 Professional Drive, Suite 249, Gaithersburg, MD 20760
24. H. K. Forsen, Bechtel Group, Inc., Research Engineering, P.O. Box 3965, San Francisco, CA 94205
25. J. R. Gilleland, GA Technologies, Inc., Fusion and Advanced Technology, P.O. Box 85608, San Diego, CA 92138
26. R. W. Gould, Department of Applied Physics, California Institute of Technology, Pasadena, CA 91125
27. R. A. Gross, Plasma Research Library, Columbia University, New York, NY 10027
28. D. M. Meade, Princeton Plasma Physics Laboratory, P.O. Box 451, Princeton, NJ 08544
29. M. Roberts, International Programs, Office of Fusion Energy, Office of Energy Research, ER-52, U.S. Department of Energy, Washington, DC 20545
30. W. M. Stacey, School of Nuclear Engineering, Georgia Institute of Technology, Atlanta, GA 30332
31. D. Steiner, Nuclear Engineering Department, NES Building, Tibbetts Avenue, Rensselaer Polytechnic Institute, Troy, NY 12181
32. R. Varma, Physical Research Laboratory, Navrangpura, Ahmedabad 380009, India
33. Bibliothek, Max-Planck Institut fur Plasmaphysik, D-8046 Garching, Federal Republic of Germany
34. Bibliothek, Institut fur Plasmaphysik, KFA, Postfach 1913, D-5170 Julich, Federal Republic of Germany

35. Bibliotheque, Centre des Recherches en Physique des Plasmas, 21 Avenue des Bains, 1007 Lausanne, Switzerland
36. Bibliotheque, Service du Confinement des Plasmas, CEA, B.P. No. 6, 92 Fontenay-aux-Roses (Seine), France
37. Documentation S.I.G.N., Departement de la Physique du Plasma et de la Fusion Controlee, Centre d'Etudes Nucleaires, B.P. 85, Centre du Tri, 38081 Cedex, Grenoble, France
38. Library, Culham Laboratory, UKAEA, Abingdon, Oxfordshire, OX14 3DB, England
39. Library, FOM-Instituut voor Plasma-Fysica, Rijnhuizen, Edisonbaan 14, 3439 MN Nieuwegein, The Netherlands
40. Library, Institute of Plasma Physics, Nagoya University, Nagoya 464, Japan
41. Library, International Centre for Theoretical Physics, Trieste, Italy
42. Library, Laboratorio Gas Ionizatti, CP 56, I-00044 Frascati, Rome, Italy
43. Library, Plasma Physics Laboratory, Kyoto University, Gokasho, Uji, Kyoto, Japan
44. Plasma Research Laboratory, Australian National University, P.O. Box 4, Canberra, A.C.T. 2000, Australia
45. Thermonuclear Library, Japan Atomic Energy Research Institute, Tokai-mura, Ibaraki Prefecture, Japan
46. G. A. Eliseev, I. V. Kurchatov Institute of Atomic Energy, P.O. Box 3402, 123182 Moscow, U.S.S.R.
47. V. A. Glukhikh, Scientific-Research Institute of Electro-Physical Apparatus, 188631 Leningrad, U.S.S.R.
48. I. Spighel, Lebedev Physical Institute, Leninsky Prospect 53, 117924 Moscow, U.S.S.R.
49. D. D. Ryutov, Institute of Nuclear Physics, Siberian Branch of the Academy of Sciences of the U.S.S.R., Sovetskaya St. 5, 630090 Novosibirsk, U.S.S.R.
50. V. T. Tolok, Kharkov Physical-Technical Institute, Academical St. 1, 310108 Kharkov, U.S.S.R.
51. Library, Institute of Physics, Academia Sinica, Beijing, Peoples Republic of China
52. N. A. Davies, Office of the Associate Director, Office of Fusion Energy, Office of Energy Research, ER-51, Germantown, U.S. Department of Energy, Washington, DC 20545
53. D. B. Nelson, Director, Division of Applied Plasma Physics, Office of Fusion Energy, Office of Energy Research, ER-54, Germantown, U.S. Department of Energy, Washington, DC 20545
54. E. Oktay, Division of Confinement Systems, Office of Fusion Energy, Office of Energy Research, ER-55, Germantown, U.S. Department of Energy, Washington, DC 20545
55. A. L. Opdenaker, Fusion Systems Design Branch, Division of Development and Technology, Office of Fusion Energy, Office of Energy Research, ER-532, Germantown, U.S. Department of Energy, Washington, DC 20545
56. W. Sadowski, Fusion Theory and Computer Services Branch, Division of Applied Plasma Physics, Office of Fusion Energy, Office of Energy Research, ER-541, Germantown, U.S. Department of Energy, Washington, DC 20545
57. P. M. Stone, Fusion Systems Design Branch, Division of Development and Technology, Office of Fusion Energy, Office of Energy Research, ER-532, Germantown, U.S. Department of Energy, Washington, DC 20545

58. J. M. Turner, International Programs, Office of Fusion Energy, Office of Energy Research, ER-52, Germantown, U.S. Department of Energy, Washington, DC 20545
59. R. E. Mickens, Atlanta University, Department of Physics, Atlanta, GA 30314
60. M. N. Rosenbluth, RLM 11.218, Institute for Fusion Studies, University of Texas, Austin, TX 78712
61. Theory Department Read File, c/o D. W. Ross, University of Texas, Institute for Fusion Studies, Austin, TX 78712
62. Theory Department Read File, c/o R. C. Davidson, Director, Plasma Fusion Center, NW 16-202, Massachusetts Institute of Technology, Cambridge, MA 02139
63. Theory Department Read File, c/o F. W. Perkins, Princeton Plasma Physics Laboratory, P.O. Box 451, Princeton, NJ 08544
64. Theory Department Read File, c/o L. Kovrizhnykh, Lebedev Institute of Physics, Academy of Sciences, 53 Leninsky Prospect, 117924 Moscow, U.S.S.R.
65. Theory Department Read File, c/o B. B. Kadomtsev, I. V. Kurchatov Institute of Atomic Energy, P.O. Box 3402, 123182 Moscow, U.S.S.R.
66. Theory Department Read File, c/o T. Kamimura, Institute of Plasma Physics, Nagoya University, Nagoya 464, Japan
67. Theory Department Read File, c/o C. Mercier, Euratom-CEA, Service des Recherches sur la Fusion Controlee, Fontenay-aux-Roses (Seine), France
68. Theory Department Read File, c/o T. E. Stringer, JET Joint Undertaking, Culham Laboratory, Abingdon, Oxfordshire OX14 3DB, England
69. Theory Department Read File, c/o K. Roberts, Culham Laboratory, Abingdon, Oxfordshire OX14 3DB, England
70. Theory Department Read File, c/o D. Biskamp, Max-Planck-Institut fur Plasmaphysik, D-8046 Garching, Federal Republic of Germany
71. Theory Department Read File, c/o T. Takeda, Japan Atomic Energy Research Institute, Tokai-mura, Ibaraki Prefecture, Japan
72. Theory Department Read File, c/o C. S. Liu, GA Technologies, Inc., P.O. Box 81608, San Diego, CA 92138
73. Theory Department Read File, c/o L. D. Pearlstein, Lawrence Livermore National Laboratory, P.O. Box 808, Livermore, CA 94550
74. Theory Department Read File, c/o R. Gerwin, CTR Division, Los Alamos National Laboratory, P.O. Box 1663, Los Alamos, NM 87545
75. H. Weitzner, Courant Institute of Mathematical Sciences, New York University, New York, NY 10012

76–235. Given distribution as shown in TID-4500, Magnetic Fusion Energy (Category Distribution UC-20g, Theoretical Plasma Physics)